Carbohydrate Polymers 321 (2023) 121280

Contents lists available at ScienceDirect

Carbohydrate Polymers

journal homepage: www.elsevier.com/locate/carbpol

Review

Alginate-metal cation interactions: Macromolecular approach

Ivan Donati [a], Bjørn E. Christensen [b,*]

[a] Department of Life Sciences, University of Trieste, Via Licio Giorgieri 5, 34127 Trieste, Italy
[b] Norwegian Biopolymer Laboratory (NOBIPOL), Department of Biotechnology and Food Science, NTNU Norwegian University of Science and Technology, Sem Sælands vei 6/8, 7491 Trondheim, Norway

ARTICLE INFO

Keywords:
Alginates
Sequence
Gelation
Solution properties
Cations
Polyelectrolyte

ABSTRACT

Alginates are a broad family of linear (unbranched) polysaccharides derived from brown seaweeds and some bacteria. Despite having only two monomers, i.e. β-D-mannuronate (M) and its C5 epimer α-L-guluronate (G), their blockwise arrangement in oligomannuronate (..MMM..), oligoguluronate (..GGG..), and polyalternating (..MGMG..) blocks endows it with a rather complex interaction pattern with specific counterions and salts. Classic polyelectrolyte theories well apply to alginate as polyanion in the interaction with monovalent and non-gelling divalent cations. The use of divalent gelling ions, such as Ca^{2+}, Ba^{2+} or Sr^{2+}, provides thermostable homogeneous or heterogeneous hydrogels where the block composition affects both macroscopic and microscopic properties. The mechanism of alginate gelation is still explained in terms of the original egg-box model, although over the years some novel insights have been proposed.

In this review we summarize several decades of research related to structure-functionships in alginates in the presence of non-gelling and gelling cations and present some novel applications in the field of self-assembling nanoparticles and use of radionuclides.

1. Introduction

Alginates are a family of polysaccharides found in several brown seaweeds from which they are produced industrially. Different species and different parts of the plants may provide alginates with different compositions. Some bacteria may produce alginates in controlled fermentation processes although commercialization of such alginates has not yet been achieved.

The ability to form hydrogels in the presence of calcium salts is beyond doubt the most studied and most utilized area in the alginate field. Calcium alginate gels have numerous applications in pharmacy, food, biotechnology and in medicine that have been reviewed by several authors over the years (Bi et al., 2022; Cao et al., 2023; Dodero et al., 2021; Hernández-González et al., 2020; Neves et al., 2020; Senturk Parreidt et al., 2018; Thiviya et al., 2023; Wang et al., 1993). Among biotechnological applications, cell encapsulation of pancreatic islets for the treatment of type-1 diabetes has been intensively studied for >40 years (Bochenek et al., 2018; Braccini & Pérez, 2001; de Vos et al., 2006). Alginates also bind other multivalent cations, some with high affinity (Hu et al., 2021), normally leading to gelation or precipitation. In contrast to the experimental simplicity of gel formation or cation exchange, the underlying physico-chemical processes are complex. They are often time-dependent and may involve the co-existence of multiple phases. The purpose of this review is to briefly recapitulate classical findings, update with newer findings and examples, and to provide a critical assessment of the current macromolecular understanding of the cation binding process.

2. Structure

Alginates comprise a rather heterogeneous family of polysaccharides (Fig. 1). Although alginates are linear (non-branched) polysaccharides containing only two different monomers, their distribution along the chain may be complex, giving rise to compositional heterogeneity. This is a result of a rather particular biosynthesis. Homopolymeric mannuronan, containing exclusively residues of β-1,4-linked D-mannuronate (hereafter abbreviated M), usually on Na^+ form, appears only as an intermediate. It is immediately processed by a family of Ca^{2+} dependent, processive C5-epimerases which convert some of the mannuronate residues to the corresponding C5 epimers, α-L-guluronate (G). This leads not only to variable G-contents, but also a non-statistical distribution of residues. The composition of alginates is therefore not adequately

* Corresponding author.
E-mail address: bjorn.e.christensen@ntnu.no (B.E. Christensen).

https://doi.org/10.1016/j.carbpol.2023.121280
Received 20 June 2023; Received in revised form 21 July 2023; Accepted 8 August 2023
Available online 9 August 2023

described only by the M/G ratio. Fortunately, standard NMR protocols provide diad (MM, MG, GM, GG) and triad (MMM, GGM.. etc.) frequencies which gives sufficient information to categorize alginates and often explain structure-dependent properties both in solution and in the gel state. A comprehensive table of the composition of algal alginates based on NMR is hereafter reported (Donati & Paoletti, 2009; Draget et al., 2006) (Table 1). Alginates with extreme compositions are rare in seaweeds but an alginate with very low G content (<10 %) can be found in fruiting bodies of *Ascophyllum nodosum*. However, pure mannuronan has become available by selectively blocking the epimerization step in bacteria (Gimmestad et al., 2003). Both mannuronan as well as other alginates can be epimerized in vitro by a range of natural and genetically engineered epimerases. This includes epimerization with an enzyme providing nearly polyalternating alginate (..MGMG..) or alginates with very high G contents (>90 %). Such alginates are valuable model substances in the study of cation binding and exchange. Bacteria of the genus *Pseudomonas* produce alginates with a very low content of G. Moreover, they always appear as single G residues. In addition, most bacterial alginates are *O*-acetylated although the acetyl groups can either be removed by alkaline hydrolysis, enzymes, or by blocking the *O*-acetylation step in the biosynthesis. The component blocks (M-blocks, MG-blocks, and G-blocks) in alginates can be isolated and purified through an elegant procedure utilizing partial hydrolysis and fractional precipitation by protonation (Haug & Smidsrød, 1968) (see also below). In fact, this classic study provided an initial proof of the 'blocky' nature of alginates, whereas the biochemical explanation (epimerases) came later.

3. Importance of G-blocks and the conformational transition from $^4C_1$ to $^1C_4$

The C5-epimerization is accompanied by a major conformational transition from the $^4C_1$ conformation of M-residues to the $^1C_4$ conformation in G-residues. Hence, the linkages of G-residues to neighboring sugars become axial rather than equatorial (as in numerous polysaccharides with β-1,4-linkages). This has several consequences: First, the linear charge density increases. Secondly, the GG motif forms a characteristic cavity (Fig. 1c and d) into which calcium ions can bind with high selectivity. This cavity and the zig-zag pattern of G-blocks form the basis for the 'egg-box' model for Ca-alginate (Fig. 1e and f) (Grant et al., 1973).

Alginates without contiguous G residues (G-blocks) have generally low selectivity for Ca^{2+} relative to Mg^{2+}. The latter cation does not lead to gelation in any type of alginate (in contrast to most other divalent cations) and has therefore been much used as an appropriate divalent reference cation.

4. Water-soluble alginates and alginic acid

Salts with monovalent cations (Li^+, Na^+, K^+ etc.) are water-soluble polyelectrolytes with little or no specific ion selectivity (Hu et al., 2021). Acidification results in carboxylate protonation whereby alginates form water-insoluble gels or precipitates. The uronic acids in alginates have as free monomers pK_a values slightly above 3 (Haug, 1964). Hence lowering pH below ca. 3 gradually converts alginates to water-insoluble alginic acid. Interestingly, the isolated component blocks display different precipitation profiles (Fig. 2): G-blocks precipitate near pH 3.5, M-blocks precipitate near pH 2, whereas MG blocks remain soluble even if fully protonated.

This property is also useful for facile counterion exchange because neutralization of precipitated alginic acid with the appropriate hydroxide provides alginate with the desired counterion. For example, neutralization with KOH provides water-soluble potassium alginate.

5. Alginates: dilute solution properties, chain expansion and stiffness

Alginates (Na^+ form) behave as semiflexible chains in aqueous

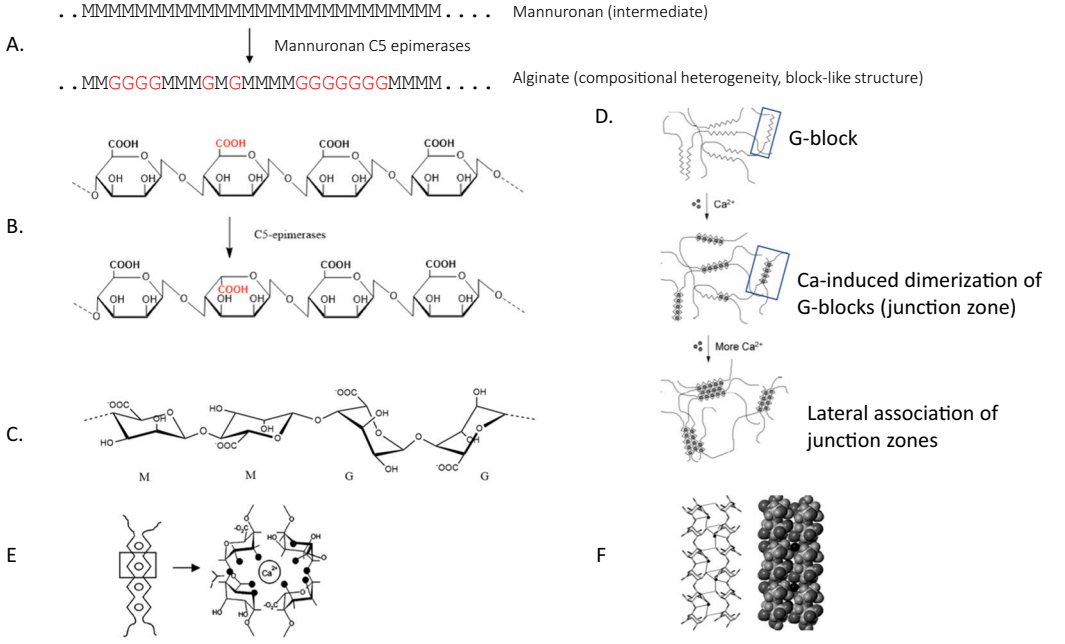

Fig. 1. Algal and bacterial alginates are obtained via the intermediate homopolymeric mannuronan (A) by the action of mannuronan C-5 epimerases, converting 4-linked-D-mannuronate (M) to L-guluronate (G) at the polymer level. Haworth formulae are given B. The resulting alginates have a blocky structure whose structure depends on the action of several epimerases. The epimerization changes the chair conformations from $^4C_1$ to $^1C_4$. G-blocks thus adopt a 'zig-zag' like helical structure witch cavities or sites which is the basis for binding of Ca^{2+} with high selectivity (C) Structures are here depicted on the acidic form (—COOH) although they are mostly used on the water-soluble, polyelectrolytic Na^+ form (—COO^- Na^+). Calcium binding is associated with chain dimerization leading to the famous egg-box structure for junction zones in calcium alginate gels (D). Reproduced from (Solberg et al., 2023) (with permission). Two detailed representations (E,F) of the "egg-box model" for Ca-alginate reproduced from (Braccini & Pérez, 2001) (with permission). See also Section 8 for details on the topic.

Table 1
Chemical composition of some algal and bacterial alginates determined by ^{1}H NMR.

Alginate source	F_G	F_M	F_{GG}	F_{MM}	$F_{GM,MG}$	F_{GGG}	F_{MGM}	$F_{GGM,MGG}$	$\overline{N}_{G>1}$
Algal									
Laminaria hyperborea (stipe)	0.63	0.37	0.52	0.26	0.11	0.48	0.07	0.05	15
Laminaria hyperborea (leaf)	0.49	0.51	0.21	0.32	0.19	0.25	0.13	0.05	8
Macrocystis pyrifera	0.42	0.58	0.20	0.37	0.21	0.16	0.17	0.04	6
Laminaria digitata	0.41	0.59	0.25	0.43	0.16	0.20	0.11	0.05	6
Lessonia nigrescens	0.41	0.59	0.22	0.40	0.19	0.17	0.14	0.05	6
Ascophyllum nodosum	0.41	0.59	0.22	0.38	0.21	0.13	0.14	0.07	5
Laminaria japonica	0.35	0.65	0.18	0.48	0.17				
Durvillaea antarctica	0.32	0.68	0.16	0.51	0.17	0.11	0.12	0.05	4
Durvillaea potatorum	0.34	0.66	0.17	0.49	0.17	0.12	0.14	0.06	4
Bacterial									
Azotobacter vinelandii	0.25 - 0.75	0.75 - 0.25	0.07 - 0.65						
Pseudomonas aeruginosa	0	1	0	1	0	0	0	0	
Pseudomonas fluorescens	0.4	0.6	0	0.2	0.4	0	0.4	0	

F_G denotes the fraction of alginate consisting of guluronic acid; F_{GG} and F_{GGG} indicate the fraction of alginate consisting of guluronic acid in blocks of dimers and trimers, respectively, whereas F_{MM} indicates the fraction of alginate consisting of mannuronic acid diads; $F_{GGM,MGG}$ indicates the fraction of alginate which starts or ends with a block of guluronic acid; $F_{GM,MG}$ indicates the fraction of alginate consisting of mixed sequences of guluronic and mannuronic acid, with F_{MGM} denoting the fraction of alginate consisting of two mannuronic acids interspaced with guluronic acid; $\overline{N}_{G>1}$ denotes the average length of guluronic acid blocks as $\overline{N}_{G>1} = (F_G - F_{MGM})/F_{GGM}$.

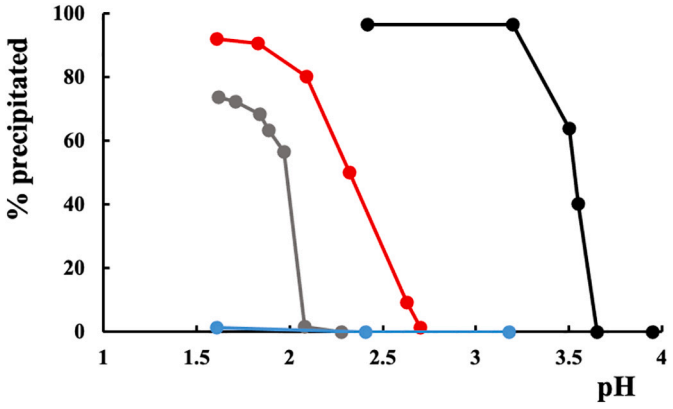

Fig. 2. pH dependent precipitation/solubility profiles of G-blocks (black), M-blocks (grey), MG-blocks (blue) as well as an alginate containing all block types (red).
(Reproduced from (Haug & Smidsrød, 1968) (with permission).)

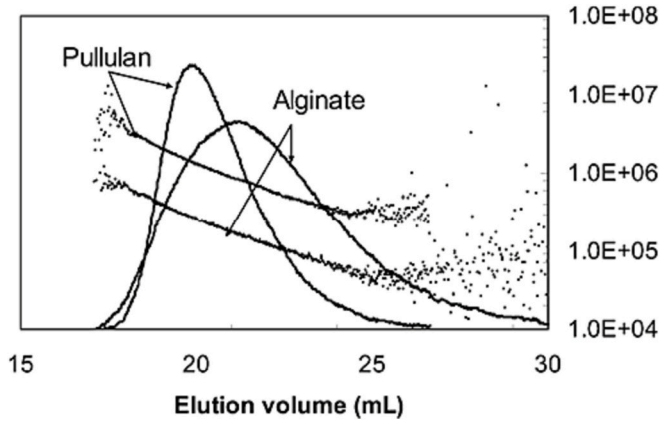

Fig. 3. SEC elution profiles (lines) and corresponding molecular weights (symbols, right axis) determined by on-line light scattering detection for alginate and pullulan. It shows that using dextran as molecular weight calibration standards would overestimate the molecular weight of alginate with a factor 4–6.
(Reproduced from (Christensen et al., 2007) (with permission).)

solution. Compared to synthetic C—C polymers they are much stiffer, a feature linked to the rigidity of the sugar residues and the restricted rotation around the 1,4-linkages. Importantly, alginates are much stiffer than dextran (Khorramian & Stivala, 1982), pullulan (Yang & Sato, 2020) (both containing flexible 1,6-linkages) or PEO (poly(ethylene oxide) (Lee et al., 2008). The three latter are commonly used as standards in size-exclusion chromatography (SEC) or gel permeation chromatography (GPC) because they are commercially available with narrow molecular weight distributions over a wide range of molecular weights. Hence, using such standards to determine molecular weights of alginates leads to an overestimation in the range 4–6 (Christensen et al., 2007) (Fig. 3).

The stiffness of alginates is within the range of other β-1,4-linked chains (chitosan, carboxymethyl cellulose), but well below those of double-stranded xanthan (Sato et al., 1984) or triple-stranded schizophyllan (Kashiwagi et al., 1981). The presence of carboxylate groups (commonly with Na^+ as counterions) adds a strongly ionic strength (and pH) dependent contribution to the expansion to the chains (Smidsrød & Haug, 1971; Vold et al., 2006) (see below for details). In the following we will review in more detail the various approaches to determine the chain stiffness of alginates and particularly examine the role of chemical composition and monomer sequence (M/G profile) in the absence of gelling cations. Based on the Odijk, Skolnick, and Fixman (OSF) theory of dilute polyelectrolyte solutions (Odijk, 1977; Skolnick & Fixman, 1977), the total persistence length, l_T, of a polyelectrolyte is the sum of the intrinsic (l_0) and electrostatic (l_e) persistence lengths (Eq. (1)):

$$l_T = l_0 + l_e \tag{1}$$

When the linear charge density of the polyelectrolyte is higher than 1 (i.e. the critical value for monovalent counterions) as in alginate, it holds (Eq. (2)):

$$l_e = \frac{1}{4 l_B \kappa^2} \tag{2}$$

where l_B is the Bjerrum length ($= e^2/(\epsilon k_B T)$, e is the electronic charge, ϵ is the dielectric constant of the bulk solvent, k_B is the Boltzmann constant, T is the absolute temperature and κ^{-1} is the Debye length (Paoletti et al., 1984).

Several authors have tackled the influence of alginate composition

on the intrinsic persistence length, l_0. Based on light scattering experiments, Smidsrød et al. argued that the presence of alternating sequences in alginate reduce the total extension of the chain (Smidsrød et al., 1973). The persistence length for alginate samples of different composition was calculated according to the following equation (Eq. (3)) (Smidsrød et al., 1973):

$$l_0 = \frac{1}{2}\left[\frac{K_\theta}{\Phi}\right]^{\frac{2}{3}}\frac{M_0}{b} \quad (3)$$

where K_θ is the constant in Flory's "equivalent sphere" viscosity theory, Φ is the Flory viscosity constant, M_0 is the monomer molar mass and b is the virtual bond length. The intrinsic persistence length, l0, was found to be 6.5–6.6 nm for alginate from *Ascophyllum nodosum* ($F_G = 9$), 7.8–8.8 for alginate from *Laminaria hyperborea* stipe ($F_G = 72.5$) and 6.5–6.9 for alginate from *Laminaria digitata* ($F_G = 38.5$), respectively.

While the values of the persistence length are quite similar, these results, combined with those obtained from an acid soluble fraction of alginate, led the authors to propose an increase in chain rigidity, in unperturbed conditions, along the sequence MG block < MM block < GG block. This was traced back to the hindered rotation around the glycosidic linkage for G residues in the $^1C_4$ conformation. Later light scattering studies combined with intrinsic viscosity measurements (a compilation of different studies was published by Vold et al. (Vold et al., 2006)) tended to give varying results. This was attributed primarily to aggregation effects and purity issues, which strongly affect light scattering results.

As an independent approach, computer simulations were used to determine the conformational maps of alginate dimers (Fig. 4a–e) (Stokke, Smidsrød, & Brant, 1993). G-G and G-M maps showed less conformational freedom with respect to M-M and M-G. A Bernoullian distribution model and a second-order Markov model allowed calculating the characteristic ratio (a stiffness parameter) for a degree of polymerization of 1000 ($<C_{1000}>$) for five different alginate samples and for mannuronan, guluronan and polyalternating, respectively. In all cases, $<C_{1000}>$ markedly varied with the fraction of guluronic residues, F_G (Fig. 4e) (Stokke, Smidsrød, & Brant, 1993). The polyalternating alginate (data point at $F_G = 0.50$) lies well below the general trend, thus providing support for the original observations discussed above.

Interestingly, the strong dependence of the calculated C_{1000} on the G-content, especially for F_G above 0.5, would imply a corresponding increase in the experimentally available radius of gyration and the intrinsic viscosity in solution (for random coils being proportional to $C_{1000}^{1/2}$ and $C_{1000}^{3/2}$, respectively), by e.g. multidetector SEC. However, experimental data (Vold et al., 2006) seem not to clearly reflect the trends seen in the modelling data. It cannot, however, be precluded some aggregation apparently occurring for the highest molecular weights (downward curvature in plots of [η] versus M, Fig. 8 in ref. (Vold et al., 2006)) contributes to mask possible stiffening effects predicted by the modelling.

Later, electron microscopy estimated a persistence length of 16 ± 7 nm for alginate with Me_4N^+ as counterion for electron optic contrast (Stokke et al., 1987). Despite the fact that during the preparation of flexible polymers for electron microscopy there is basically a change in conformation from three-dimensional to two-dimensional arrangement that might affect the information on polymer-chain flexibility, still this evaluation is in line with other measurements.

The [η]-M data for different alginates obtained by SEC-MALLS were further used to determine the total persistence length (l_T) at $I = 0.17$ M using the Bohdanecký approach (Vold et al., 2006), yielding:

Mannuronan: $l_T = 14.5 \pm 1.8$ nm;

Guluronan ($F_G > 0.85$): $l_T = 16.5 \pm 0.5$ nm.

Polyalternating: $l_T = 14.9 \pm 1.2$ nm.

Additionally, the same authors determined the persistence length at infinite ionic strength (i.e. screening of long range electrostatic interactions) concluding that l_0 of alginate, both natural and enzymatically epimerized, is around 12 nm (Vold et al., 2006). This is also reflected in the relationship between the radius of gyration of alginate samples and the molecular weight which, regardless the composition, reads (Vold et al., 2006) (Eq. (4)):

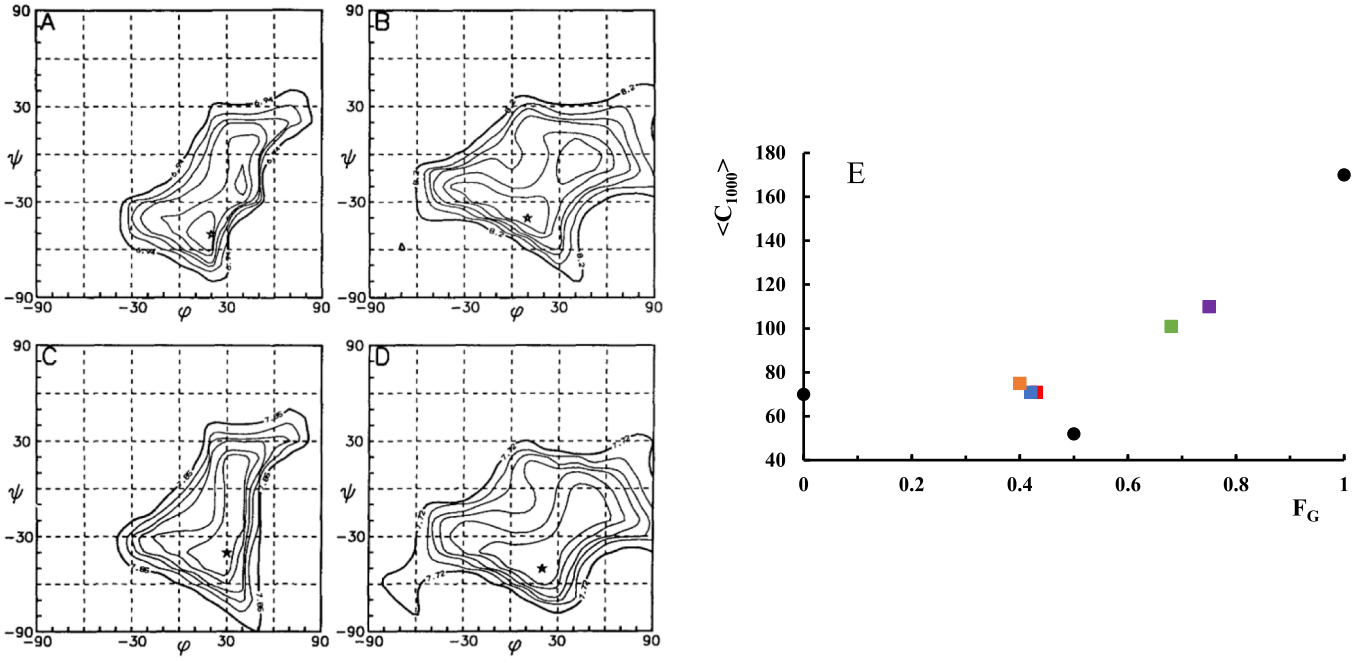

Fig. 4. (A–D) Iso-energy contour plots of the conformational energies for the G-G (A), M-M (B), G-M (C) and M-G (D) dimers occurring in alginates. The contours are drawn at +0–5, +1, +2, +3, +5 and +10 kcal/mol above the respective minima denoted with a star. Reproduced with permission from (Stokke, Smidsrød, & Brant, 1993). E) Characteristic ratio (at DP 1000 $<C_{1000}>$) versus F_G for alginates isolated from *A. nodosum* (red), *M. pyrifera* (blue), *L. digitata* (orange), *L. hyperborea* (green) and L. *hyperborea* outer cortex (purple). Black dots represent the characteristic ratio calculated for polyalternating, mannuronan and guluronan. Replotted from (Stokke, Smidsrød, & Brant, 1993) (with permission).

$$\langle R_G \rangle \propto M_w^{0.60} \quad (4)$$

Similarly, regardless the origin of the alginate sample, the Mark-Houwink-Sakurada reads:

$$20\,000 < M < 100\,000 : [\eta] = 0.0051\, M^{1.00}$$

$$100\,000 < M < 300\,000 : [\eta] = 0.0349\, M^{0.83}$$

$$300\,000 < M < 1\,000\,000 : [\eta] = 0.0305\, M^{0.66}$$

Similar experiments were performed on ultra-high molar mass alginate samples extracted from L. *trabeculata* and *L. nigrescens* by Storz et al. (Storz et al., 2009). Despite a F_G ranging from 0.78 to 0.39, samples showed a common Mark-Howink-Sakurada semi-empirical parameters, both for native and ultrasonically degraded samples in the M_w range $3 \cdot 10^5$–$1 \cdot 10^6$ (Eq. (5)):

$$[\eta] = 0.059\, M_w^{0.78 \pm 0.02} \quad (5)$$

The following relationship was found to hold regardless the composition (Eq. (6)).

$$\langle R_G \rangle \propto M_w^{0.52-0.53} \quad (6)$$

In fact, when overlaid by the data of Vold et al. (Vold et al., 2006) the two data sets are nearly indistinguishable. Slightly different exponents can be explained by the two-parameter fit used to provide the parameters: Higher exponents are 'compensated' by lower pre-exponential factors.

6. Alginate as polyelectrolyte. Monovalent counterions

Alginate is commonly used, in all applications, as sodium salt (sodium alginate). Very little work has been carried out on the interaction between alginate and monovalent ions since there is limited practical application of such systems. It has been reported that CD spectra of alginate are affected by the presence of different monovalent cations, with lower ellipticity values detected for larger or smaller cations ($Li^+ < Na^+ < K^+ > Rb^+ > Cs^+ > NH_4^+$) (Seale et al., 1982). This behavior is sequence specific, being more marked for polyguluronan than for polymannuronan, and requires quite concentrated solutions of monovalent ion (0.5 M), while it is not noticed at lower ion concentrations (Donati et al., 2006). Molecular simulations show a very similar distribution of K^+ and Na^+ ions around the alginate chain, leading to a similar density and tightness of the counterion atmosphere (Perić-Hassler & Hünenberger, 2010). However, the same simulations found a higher frequency of ion-binding events for K^+ with respect to Na^+ (Perić-Hassler & Hünenberger, 2010). Molecular dynamics simulations show that the interaction of a guluronan chain with Na^+ is equivalent to that of Ca^{2+} but less stable. However, the modelling of the interactions between Na^+ counterions and two guluronan strands show a more transient nature. No chain-chain aggregation was observed, likely because Na^+ ions localization deep in the binding pocket prevents the accessibility to a second polyelectrolyte chain (Stewart et al., 2014a). Similar conclusion was drawn for mannuronan and polyMG with Na^+ (Stewart et al., 2014b).

From the theoretical point of view, the distribution of monovalent ions around the alginate chain can be described in terms of the Poisson-Boltzmann or of the Manning's Counterion Condensation (CC) theory. As to the latter, the linear charge density of a polyelectrolyte, ξ, is defined as (Eq. (7)):

$$\xi = \frac{l_B}{b} \quad (7)$$

where b is the structural distance, projected along the helix axis, between monovalent charges on the polymer backbone.

All in all, predictions obtained from the Poisson-Boltzmann cell model on the fraction of Na^+ ions unspecifically bound are in line with the fraction of condensed counterions calculated by means of the Manning's limiting theory (Grasdalen & Kvam, 1986). Focusing on Na^+ ions, the unspecific binding to alginate chains was nicely shown by Grasdalen and Kvam using ^{23}Na NMR line width. Specifically, upon addition of a tetramethyl ammonium salt of alginate, $^{23}Na^+$ ions in solution are unspecifically bound in the region close to the polyelectrolyte chain, increasing the line-width of their NMR signal (Fig. 5). This experiments pointed to an exchange of Na^+ ion between a bound and a free state (Grasdalen & Kvam, 1986).

The fraction of unspecifically bound Na^+ ions shows a slight dependence from alginate concentration and differs on the basis of the linear charge density of the polyelectrolyte, i.e. guluronan from mannuronan (Grasdalen & Kvam, 1986). However, even the lowest polymer concentration tested shows an appreciable fraction of unspecifically bound monovalent counterions, in contrast with prediction from the mass-action law. The use of the CC theory allows predicting the fraction of monovalent counterions in the condensation volume, r, on the basis of the linear charge density of guluronan, mannuronan and polyalternating (Donati et al., 2006):

Guluronan: $b_{str} = 4.35$ Å; $\xi = 1.64$; $r = 0.39$.
Mannuronan: $b_{str} = 5.17$ Å; $\xi = 1.38$; $r = 0.275$.
Polyalternating: $b_{str} = 4.76$ Å; $\xi = 1.50$; $r = 0.33$.

NMR measurements allow determining the onset for the unspecific binding of Na^+ ions as a sudden increase in its relaxation rate. Starting from a protonated mannuronan, unspecific Na^+ binding takes place at a degree of neutralization that causes the linear charge density of the polyelectrolyte to exceed the critical value predicted by Manning's CC theory. In addition, CC theory has shown a good ability to predict the enthalpy of mixing of mannuronan with Na^+ counterions (Donati et al., 2006).

7. Alginate as polyelectrolyte. Non-gelling divalent counterions

Mg^{2+} is generally recognized as a non-gelling ion, although the use of a very high ion and polymer concentration could (reversibly) lead to structures that are insoluble in water (Topuz et al., 2012). Smidsrød et al. described Mg^{2+}-polyuronates systems like a milky precipitates rather than proper hydrogels (Smidsrød & Haug, 1972).

Minor modifications in the CD spectra and in light scattering are measured for Mg^{2+}-alginate with respect to Na^+-alginate (Donati, Asaro, & Paoletti, 2009; Thom et al., 1982). ^{13}C NMR showed that Mg^{2+} ions bind weakly to alginate without a preferred binding site, which correlates with the fact that no macroscopic gelation occurs (Lattner et al., 2003). Ca^{2+} and Mg^{2+} showed no differences as to binding to a single guluronan chain according to molecular dynamics studies. However, a prevailing effect of calcium over magnesium binding was observed

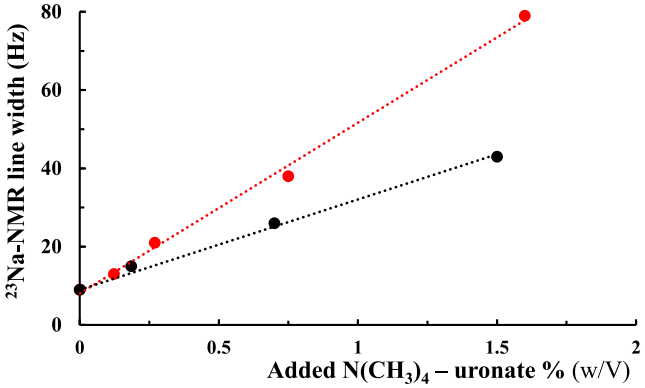

Fig. 5. ^{23}Na NMR line widths produced by addition of tetramethylammonium alginates. Red dots represent an alginate sample with $F_G = 0.5$ and $F_{GG} = 0.3$; black dots represent mannuronan sample (Mw ~ 670,000).
(Replotted from (Grasdalen & Kvam, 1986) (with permission).)

when mixtures of the two ions were used (Perić-Hassler & Hünenberger, 2010). Strikingly, the ranking of ion binding on a single guluronan chain, in the absence of affinity contributions, was $K^+ > Na^+ > Ca^{2+} > Mg^{2+}$.

The decrease in specific viscosity in dilute solution showed that Mg^{2+} condensation varied for different sequences in alginate, increasing along the series mannuronan < polyalternating < guluronan (Donati, Asaro, & Paoletti, 2009). These results suggested the presence of a free energy of affinity, ΔG_{aff}, for the Mg^{2+} ion, which depends on the alginate sequence (Fig. 6).

The effect of Mg^{2+} ions on polyuronates has also been studied using different theoretical approaches. Savitsky et al. proposed a modified Poisson-Boltzmann cell model to describe a polyuronate (polygalacturonate) salt with a divalent cation, specifically Mg^{2+}, as counterion (Qian et al., 1989). Mg^{2+} ion displaced Na^+ ions, as seen by means of ^{23}Na NMR, increasing also its condensation on the polyelectrolyte with a polymer concentration dependence. However, experimental and theoretical fractions of territorially bound Mg^{2+} ions on the polyuronate differ quite substantially (Riedl et al., 1989).

Donati et al. exploited the Manning's CC theory to describe alginate in a mixture of Na^+ and Mg^{2+} ions (Donati et al., 2006; Donati, Asaro, & Paoletti, 2009). Both ions are present in the condensation volume in the proximity of the polyelectrolyte, thus reducing its effective charge. Given the linear charge density of alginates of different compositions, the condensation of Mg^{2+} varied for mannuronan, polyalternating and guluronan (Fig. 7a). The higher the linear charge density of alginate, the higher the fraction of condensed Mg^{2+} ion, $r_{Mg^{2+}}$, thus displacing the Na^+ ion. The introduction, in the theoretical framework of the CC theory, of a contribution arising from the free energy of affinity, ΔG_{aff}, accounted for a specific effect of the Mg^{2+} ion on alginate sequences (Fig. 7b). The larger is the "excess" free energy of affinity, the larger is the fraction of Mg^{2+} ion in the condensation volume.

ΔG_{aff} increased along the sequence MM < MG < GG. The predictions based on the Counterion Condensation theory for the variation of the fraction of condensed Na^+ ions, Δr_{Na^+}, upon addition of Mg^{2+} are in qualitative good agreement with the variation of the relaxation rate of sodium ions, ΔR_{Na^+}, determined by ^{23}Na NMR (Fig. 8) (Donati, Asaro, & Paoletti, 2009).

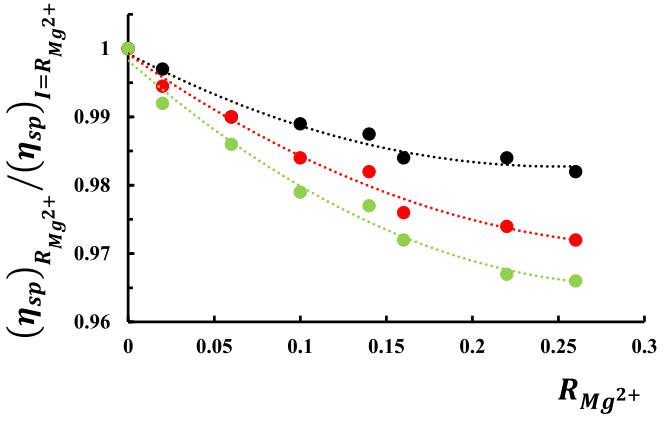

Fig. 6. Dependence on $R_{Mg^{2+}}$ of the specific viscosity ratio ($(\eta_{sp})_{R_{Mg^{2+}}} / (\eta_{sp})_{I=R_{Mg^{2+}}}$) for mannuronan (black), polyalternating (red) and guluronan (green). $R_{Mg^{2+}}$ refers to the ratio between the concentration of Mg^{2+} ions ($[Mg^{2+}]$) and polymer concentration expressed in monomol/L (Cp) with $R_{Mg^{2+}} = [Mg^{2+}]/Cp$. $(\eta_{sp})_{R_{Mg^{2+}}}$ refers to the specific viscosity of the polyelectrolyte solution at each $R_{Mg^{2+}}$ value while $(\eta_{sp})_{I=R_{Mg^{2+}}}$ refers to the specific viscosity of the polyelectrolyte solution at an ionic strength (I) equaling the one obtain at each $R_{Mg^{2+}}$ but with Na^+ ions. Redrawn from (Donati, Asaro, & Paoletti, 2009) (with permission).

8. Alginate as polyelectrolyte. Gelling divalent ions

The cooperative mechanism of Ca^{2+} ion binding that involves two or more alginate chains is described using the so-called "egg-box model" (Fig. 1) (Grant et al., 1973). The analogy is made with the "comfort with which eggs of the particular size may pack in the box" (Grant et al., 1973). The binding of Ca^{2+} ion involves a four-oxygens coordination and a 2_1 helical conformation of the polymer chain packed in hexagonal lattice with a constant of 0.66 nm (Sikorski et al., 2007). The role of the different sequences along the chain has been explored over the years. The fundamental contribution in the ion binding by G-blocks has been recognized by Haug and Smidsrød and the following ion affinity series was reported $Pb^{2+} > Cu^{2+} > Cd^{2+} > Ba^{2+} > Sr^{2+} > Ca^{2+} > Co^{2+}$, Ni^{2+}, $Zn^{2+} > Mn^{2+}$ (Haug & Smidsrød, 1970; Smidsrød & Haug, 1972). Mørch et al. reinterpreted the affinity of the different sequences in alginate for some divalent cations as follows (Mørch et al., 2006):

GG-blocks: $Ba^{2+} > Sr^{2+} > Ca^{2+} >> Mg^{2+}$
MM-blocks: $Ba^{2+} > Sr^{2+} \sim Ca^{2+}$
MG-blocks: $Ca^{2+} > Sr^{2+} \sim Ba^{2+}$

The elucidation of the egg-box model has been obtained by means of X ray diffraction studies, pointing to a 2_1 conformation for the G blocks in the Ca^{2+}-junctions (Sikorski et al., 2007). The formation of dimers by the coordination of the cation prevents further lateral packing, while Na^+, Ca^{2+}, water molecules and hydrogen bonding mediate disordered associations. Molecular modelling established the validity of the egg-box model for Ca^{2+} binding, where the most favorable antiparallel associations of the polyelectrolyte chains can be regarded as a "shifted egg box", with a limited effect on the structure (Braccini & Pérez, 2001).

The role of the length of the G-blocks in calcium binding has been studied over the years. Pioneering work by Kohn showed that activity coefficient of Ca^{2+} ion has an abrupt decrease when the degree of polymerization is around 18 for oligoguluronates, while it basically follows the theoretical curve for oligomannuronan (Fig. 9) (Kohn, 1975). The latter was calculated considering a purely electrostatic interaction between the ion and the polyuronates. The marked deviation from the theoretical behavior pointed to a inter chain binding rather than an intra chain binding of the ion (Kohn, 1975).

A theoretical model based on cooperative binding and gel leaching studies estimated in DP8 the minimum length of oligoguluronate required to form a stable egg-box junction corresponded (Stokke et al., 1991; Stokke, Smidsrød, Zanetti, et al., 1993). AFM and DFM recently confirmed this estimation and provided evidence that the release of internal stresses generated by constraints due to competing crosslinks could take up to several hundred milliseconds (Bowman et al., 2016). Studies of relaxation on alginate hydrogels revealed the existence of long-lived (egg-box junctions) and shorter-lived (single cross-linking points) bonds, both contributing to the overall mechanical properties (Larobina & Cipelletti, 2013).

Different authors described the initial binding of Ca^{2+} by alginate chains. Fang et al. proposed in 2007 a multiple step mechanism on the basis of viscosimetric and calorimetric measurements. This foresees the binding of calcium ions on single alginate chains prior to the formation of egg-box structures involving two alginate strands (Fang et al., 2007). A ratio $[Ca^{2+}]$/[guluronic acid] of 0.25, i.e. the ideal ratio found in the egg-box, is the onset of interchain association.

Molecular dynamic and Monte Carlo simulations described the initial binding of calcium ions by two strands of guluronan, with the cation embedded in a pocked coordinating four oxygen atoms on one chain and the carboxylate oxygen on the second polyuronate chain, together with three water molecules. According to this study, the two polyuronate chains are envisaged in an approximate perpendicular arrangement (Stewart et al., 2014a). The latter resembles the open 3D alginate networks seen by AFM (Decho, 1999).

Borgogna et al. in 2013 proposed an alternative model for the description of the initial Ca^{2+} binding by alginate based on viscosimetric determinations similar to those of Fang et al. (Borgogna et al., 2013).

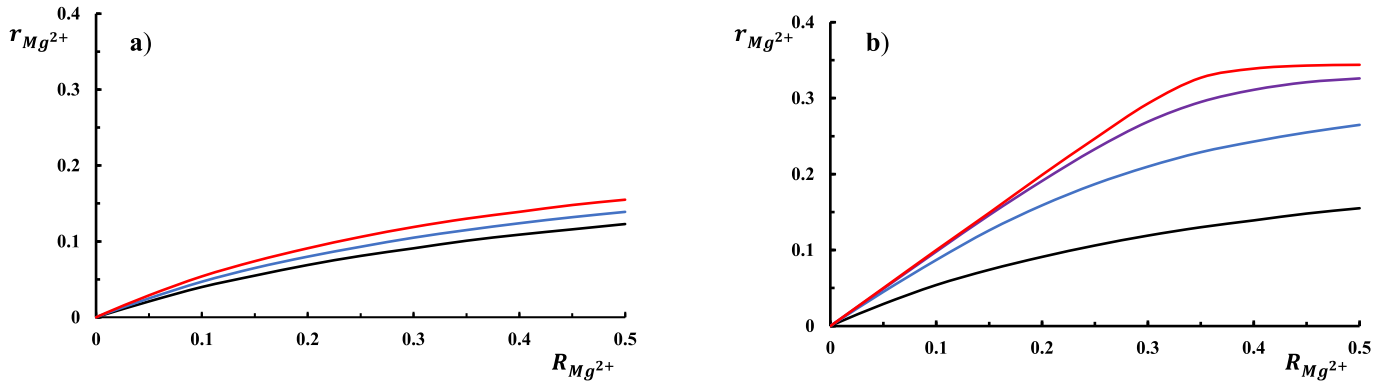

Fig. 7. **a**) Dependence of the fraction of condensed Mg^{2+} ions, $r_{Mg^{2+}}$ from $R_{Mg^{2+}}$ (see caption to Fig. D for definition) for mannuronan (black), polyalternating (blue) and guluronan (red), respectively. **b**) Dependence of the fraction of condensed Mg^{2+} ions, $r_{Mg^{2+}}$, from $R_{Mg^{2+}}$ for Guluronan with an excess free energy of affinity, ΔG_{aff}, of 0 (black), − 6 kJ mol^{-1} (blue), − 10 kJ mol^{-1} (violet), and − 14.9 kJ mol^{-1} (red). Calculations preformed with a polymer concentration (Cp) of $3.5 \cdot 10^{-3}$ monomol/L and supporting salt (NaCl) = 0.05 M.

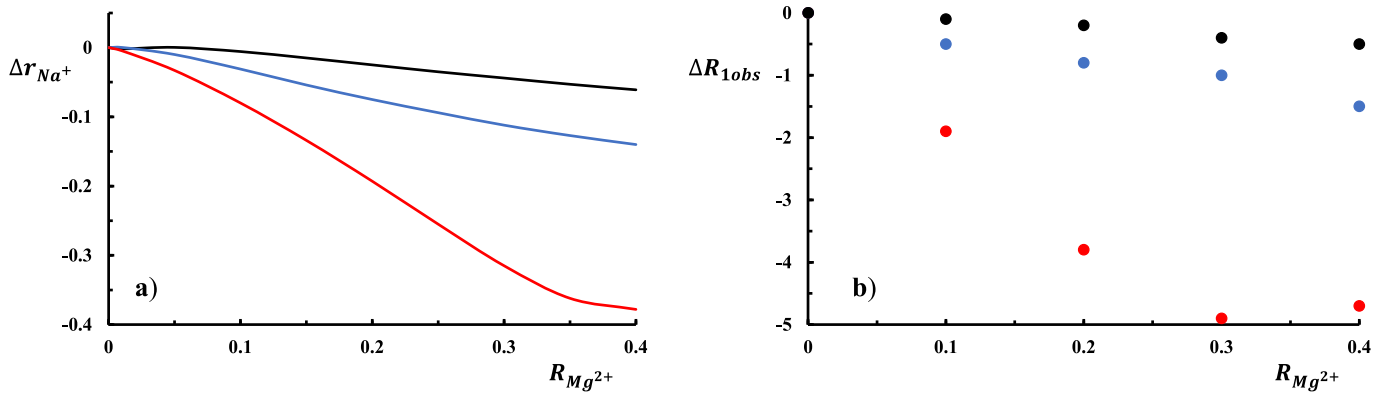

Fig. 8. Dependence of **a**) the variation of the fraction of condensed Na^+ ions, Δr_{Na^+} and of **b**) the variation of the relaxation rate of Na^+, ΔR_{1obs} from $R_{Mg^{2+}}$ (see caption to Fig. D for definition) for mannuronan (black), polyalternating (blue), and guluronan (red). In **a**), ΔG_{aff} was set to 1.26 kJ·mol^{-1} for mannuronan, 4.94 kJ·mol^{-1} for polyalternating and 14.9 kJ·mol^{-1} for guluronan, respectively.
(Redrawn from (Donati, Asaro, & Paoletti, 2009) (with permission).)

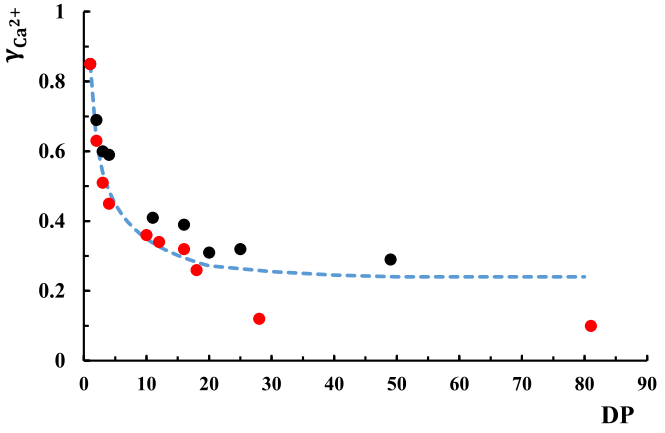

Fig. 9. Activity coefficient of Ca^{2+}, $\gamma_{Ca^{2+}}$, in solution of calcium mannuronan (black) and guluronan (red), respectively, as a function of the degree of polymerization (DP). The dashed blue line represents the theoretical $\gamma_{Ca^{2+}}$ values calculated for pure electrostatic interaction of Ca^{2+} with carboxylic groups of oligomannuronan.
(Reproduced from (Kohn, 1975) (with permission).)

According to this model, four G residues in two guluronan strands bind Ca^{2+} (interchain binding) in the so-called "tilted" egg-box arrangement. This causes a decrease in the specific viscosity (Fig. 10). Due to geometrical and electrostatic (like-charge repulsion) considerations, the alginate chains emerging from the tilted egg-box are not parallel but are placed at an angle close to 90°. Although the calcium ion brings together two alginate chains, the geometrical order deviates sensibly form the egg-box structure. Upon further additions of calcium, the "tilted" egg-box evolves in the "classic" egg-box through the clustering of cross-links along the alginate chains in a mechanism that resembles the so-called "railway track" (Borukhov et al., 2002), causing an upturn in the specific viscosity.

Stokke et al., using AFM measurements, found in 2016 sharp rupture points upon stretching oligoguluronate chains treated with calcium ions (Bowman et al., 2016) These were considered consistent with the perpendicular cross-linking mechanism proposed independently by both Stewart and Borgogna (Borgogna et al., 2013; Stewart et al., 2014a).

Recently, a thermodynamic approach described the initial binding of Ca^{2+} ions by alginate chains using two binding modes which interconvert: an initial binding type (type-1) corresponding to the tilted egg-box that, upon further addition of calcium, evolves in a second binding type (type-2) corresponding to the formation of geometrically ordered egg-box structures (Paoletti & Donati, 2022). For the first additions of Ca^{2+} to the alginate solution, the tilted egg-box binding mode takes place to an extent larger than the statistical predictions. Upon increasing the amount of calcium, the tilted egg-box is converted in the perfect,

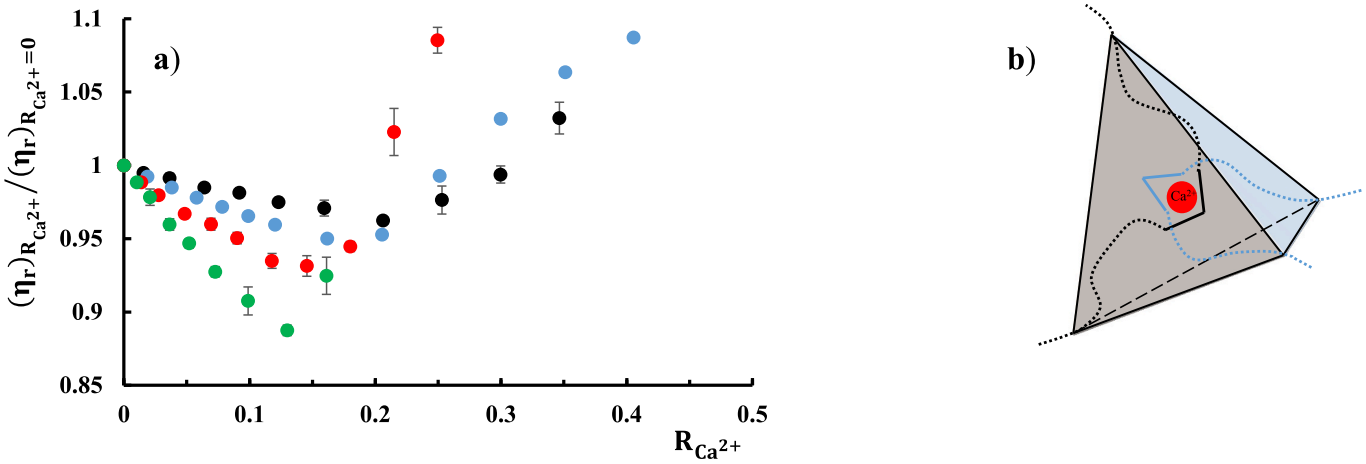

Fig. 10. **a**) Dependence on $R_{Ca^{2+}}$ of the relative viscosity ratio $((\eta_r)_{R_{Ca^{2+}}}/(\eta_r)_{R_{Ca^{2+}}=0})$ for alginate from L. *hyperborea* in aqueous NaCl 0.05 M at a polymer concentration of 0.5 g/L (black), 0.7 g/L (blue), 1 g/L (red), and 1.4 g/L (green), respectively. $R_{Ca^{2+}}$ refers to the ratio between the concentration of Ca^{2+} ions ($[Ca^{2+}]$) and polymer concentration expressed in monomol/L (Cp) with$R_{Ca^{2+}} = [Ca^{2+}]/Cp$. $(\eta_r)_{R_{Ca^{2+}}}$ refers to the relative viscosity of the polyelectrolyte solution at each $R_{Ca^{2+}}$ value while $(\eta_r)_{R_{Ca^{2+}}=0}$ refers to the relative viscosity of the polyelectrolyte solution prior to the addition of Ca^{2+}. Redrawn from (Borgogna et al., 2013). **b**) Graphical representation of the "tilted egg-box". Red circle represents a Ca^{2+} ion. Redrawn from (Borgogna et al., 2013).

ordered egg-box (type-2). However, the amount of calcium required for the onset of the perfect egg-box is larger than what predicted by the statistical distribution of ions along the chain, thus reflecting the cooperativity of the process (Fig. 11).

MG sequences show the ability to bind calcium ions, although the role of the G blocks in alginate prevails. Smidsrød and Haug already in 1972 suggested the potential involvement of MG-blocks in the formation of junctions with Ca^{2+} ions (Smidsrød & Haug, 1972). In 1999, it was also suggested that mannuronic residues could bind Ca^{2+} when neighbored by a guluronic group (Wang et al., 1993). Donati et al. in 2005 reported the first example of Ca^{2+} binding by MG sequences and this led to three potential junctions involving G- and/or MG-blocks in alginate (Fig. 12) (Donati et al., 2005).

The Ca^{2+} binding ability of polyMG was studied by means of molecular dynamics simulation. Two polyMG strands bind Ca^{2+} in a V-shaped motif with an angle of about 60° and the interchain interaction is mediated by a carboxylate-ion-carboxylate bridging. The interactions of MG strands with Ca^{2+} are somewhat similar to those shown by polyG and thus their involvement in the alginate Ca^{2+}-hydrogel network is considered likely.

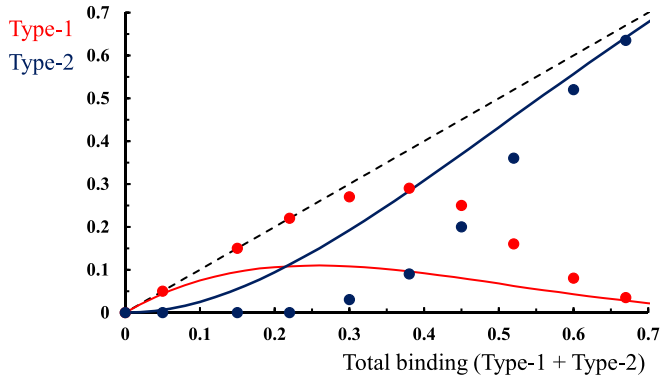

Fig. 11. Dependence of the fraction of Type-1 (Tilted egg-box, red dots) and Type-2 (ordered egg-box, blue dots) calcium binding modes in alginate from the total fraction of bound calcium ions (total binding). The dotted black line represents the total binding limit. The continuous lines represent the fraction of Type-1 (red) and Type-2 (blue) calcium binding modes calculated assuming a purely statistical filling up of sites with no interaction among nearest-neighboring sites.
(Replotted from (Paoletti & Donati, 2022).)

9. Alginate hydrogels

9.1. Acid gels

Semidilute alginate solutions can form acid hydrogels, stabilized by hydrogen bonding, when the pH of the solution is lower than the pK_a of the uronic acid. Mechanical properties of alginic acid hydrogels become independent from pH below 2.5 and depend on polysaccharide composition, with G-rich alginates showing a 6-fold increase in Young's modulus with respect to M-rich ones (Draget et al., 1994). The gel strength of alginic acid hydrogels shows the following power law dependence from polymer concentration: $E \propto c^{1.5}$ (Draget et al., 1994). Alginic acid hydrogels show no swelling at pH $\leq$ 2 and a complete dissolution at pH $\geq$ 4.5, while at pH 4 the swelling capacity decreases with increasing amount of G residues (Draget et al., 1996). SAXS studies showed that, in the case of alginic acid, gelation takes place with an initial phase formed by quasi-ordered junction zones composed of 3–4 laterally associated chains and a second phase where junction zones assemble in domains of about 5 nm. The length of the junction zones correlated with the fraction of GM sequences in the polysaccharide chains (Draget et al., 2003).

9.2. Ionic gels

The treatment of semidilute and concentrated sodium-alginate solutions with proper divalent ions, such as Ca^{2+}, leads to the formation of ionotropic hydrogels. The gelation process is based on the higher affinity of alginate for divalent ions than for monovalent ones. Smidsrød argued that the affinity towards a specific divalent ion increases upon increasing its content in the medium through a near-neighbor auto-cooperative process (Smidsrød, 1974). Depending on the method used for the introduction of the cross-linking ion in the alginate solution, homogeneous or inhomogeneous hydrogels are obtained (Fig. 13).

9.3. Homogeneous alginate hydrogels

Controlled and homogeneous delivery of Ca^{2+} ions to solutions of Na-alginate is a non-trivial challenge. The almost instantaneous reaction leads to inhomogeneities that tend to persist over time. To circumvent this problem methods for more homogeneous Ca delivery have been

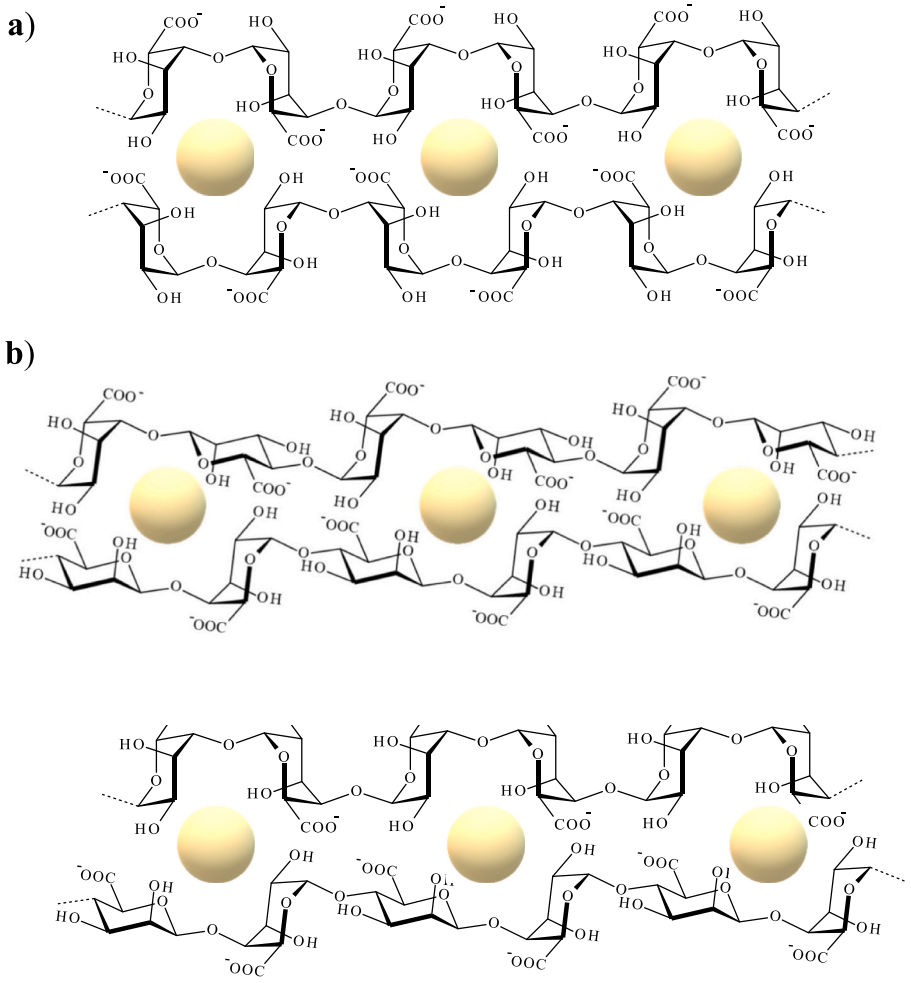

Fig. 12. Graphical description of the three potential junctions in Ca^{2+}-alginate gels. a) GG/GG junctions, b) MG/MG junctions, and c) GG/MG junctions. (Redrawn from (Donati et al., 2005).)

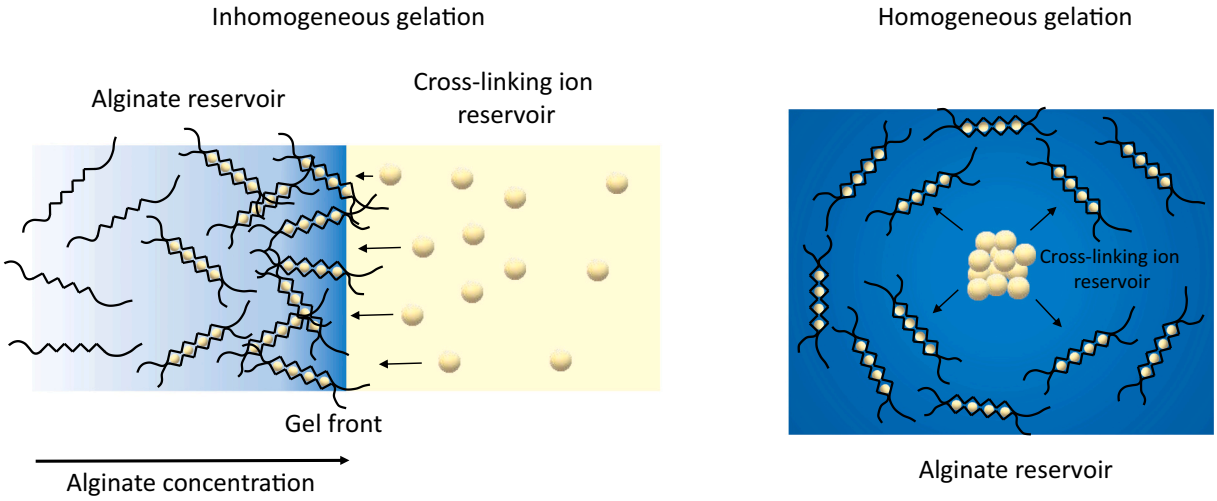

Fig. 13. Homogeneous and Inhomogeneous gelation of alginate.

explored. Current methods rely on evenly distributing Ca^{2+} as either insoluble $CaCO_3$ (finely ground particles) or as bound to a chelator such as EGTA, to the Na-alginate solution. During mixing, which occurs near neutral pH, little Ca is released. Therefore, the slowly hydrolyzing GDL (glucono-δ-lactone) is added, whereby pH gradually decreases. Protons are partly consumed by either $CaCO_3$ ($CaCO_3 + 2H^+ = Ca^{2+} + 2HCO_3^-$) or EGTA (protonation releases Ca^{2+}), and the homogeneously released Ca^{2+} reacts with the alginate (Draget et al., 1990). While a good homogeneity, on the mm scale, is achieved and the final pH of the construct is neutral, the hydrolysis of GDL significantly reduces the local

pH to displace Ca^{2+} from the chelator. This limits the applications of this methodology for cell encapsulation.

A more elaborate version involving several chelators has been developed for the preparation of Ca-alginate microbeads by means of microfluidics (Bassett et al., 2016). Here, two chelators are used in combination with two divalent cations (Fig. 14). The selectivities for the two cations are different for the two chelators, and selected in such a way that mixing two homogeneous alginate solutions leads to cation exchange: The chelator bound to Ca^{2+} has higher selectivity for the other ('exchange') ion, for example Zn^{2+}, but the other chelator (bound to Zn^{2+}) has lower Ca^{2+} selectivity than the alginate. Hence, Ca^{2+} is released and allowed to react with the alginate, whereas the exchange ion becomes bound to the chelator originally being bound to Ca^{2+}. This strategy enables control of ion release kinetics within an aqueous polymer solution and thus control over gelation kinetics across a wide range of pH.

The CLEX approach allows reaching a good control over gelation kinetics and viability of eukaryotic and prokaryotic cells (Bassett et al., 2016; Håti et al., 2016; Yamamoto et al., 2019).

The use of highly soluble calcium salts, such as $CaCl_2$, prevents the formation of a homogeneous alginate hydrogel given the instantaneous release of Ca^{2+} ions in solution. A calcium salt with limited solubility, such as $CaSO_4$, overcomes this limitation: the slower release of Ca^{2+} ions, with respect to $CaCl_2$, allows a homogeneous mixing and a casting of the alginate suspension before the completion of the gelation. This approach shows several advantages when applied to the inclusion of cells within 3D alginate-based hydrogel (Chaudhuri et al., 2015). However, a deeper analysis on the homogeneity is needed before reliable protocols are developed.

An additional approach to obtain homogeneous alginate gels requires the presence, in the cross-linking solution, of a non-gelling competing ion in high concentration, such as Na^{+}. In this case, the binding of the cross-linking ion is slowed down and a homogeneous diffusion of Ca^{2+} ion throughout the alginate solution is accomplished (Strand, Mørch, Espevik, & Skjåk-Bræk, 2003).

9.4. Inhomogeneous alginate hydrogels

The use of a diffusion setting approach leads to inhomogeneous alginate hydrogels. In this case, the cross-linking ions are allowed to diffuse from an outer reservoir into an alginate solution. Due to the rapid ion binding and gel formation, alginate is driven towards the gelling front and the final result is an uneven distribution of the polysaccharide along the network (Skjåk-Bræk et al., 1989). This kinetically driven gel formation can lead to a fivefold increase in alginate concentration at the gelling front with respect to the starting polysaccharide solution. The result is a compact outer layer and a soft liquid core in the central part of the 3D network. The inhomogeneity of alginate hydrogels has been confirmed by several experimental techniques, such as synchrotron radiation induced X-ray emission, MRI, Raman spectroscopy and confocal microscopy (Heinemann et al., 2005; Strand, Mørch, Espevik, & Skjåk-Bræk, 2003; Thu et al., 2000). More recently, confocal laser scanning microscopy and confocal Raman microscopy confirmed the inhomogeneous distribution of alginate within hydrogels and the marked increase in polysaccharide concentration at the gelling front (Kroneková et al., 2018). SAXS experiments revealed a strongly anisotropic structure with a molecular orientation perpendicular to the gelation direction, which decreased upon increasing the distance from the gelation front (Maki et al., 2011). In addition, a multichannel structure, with capillary axis aligned towards the gel growth direction, was reported (Thumbs & Kohler, 1996). Photon Correlation Imaging shows a quasi-instantaneous process of hydrogel formation upon contact between the alginate solution and the Ca^{2+} reservoir and an advancement of the gelation front at a speed of 0.3 mm h^{-1} (Secchi et al., 2013).

Alginate concentration and molecular weight, as well as the cross-linking ion, determine the polymer gradient within inhomogeneous hydrogels. A low molecular weight alginate leads to more inhomogeneous hydrogels. Conversely, high molecular weight alginate increases the homogeneity of the network. The increase in the concentration of the cross-linking ions enhances the diffusion of the ion within the network and the alginate gelation takes place contemporary in the outer and inner part of the alginate solution, leading to more homogeneous hydrogels (Mørch et al., 2006). The same effect is obtained upon increasing alginate concentration which, by increasing the viscosity of the system, limits the migration of the polysaccharide towards the gelling front. In general terms, the higher the inhomogeneity of the alginate gel the lower its porosity and swelling (Martinsen et al., 1992; Skjåk-Bræk et al., 1989; Thu et al., 1996).

While the composition of alginate, in terms of block structure, only partially affects the inhomogeneity of hydrogels, the divalent ion selected for reticulation is relevant. The replacement of Ca^{2+} with Ba^{2+} leads, in fact, to more inhomogeneous hydrogel, likely due to the higher affinity of the latter over the former for the alginate chains. The inhomogeneity of alginate hydrogel is also increased when it is treated with a polycation, such as poly-L-lysine, regardless of the ion used in the primary network formation (Strand, Mørch, Syvertsen, et al., 2003).

9.5. Mechanical properties

Synthetic polymer networks are adequately described using the rubber elasticity theory (Flory, 1953; Treloar, 2005). The elasticity of the polymer network arises from the loss in conformational entropy of the polymer chains between reticulation points upon stretching. For an ideal rubber, it holds (Eq. (8)):

$$\frac{\sigma}{\gamma} = G = NkT = \frac{c_p}{M_c} RT \tag{8}$$

where σ and γ are the shear stress and strain, respectively, G is the shear

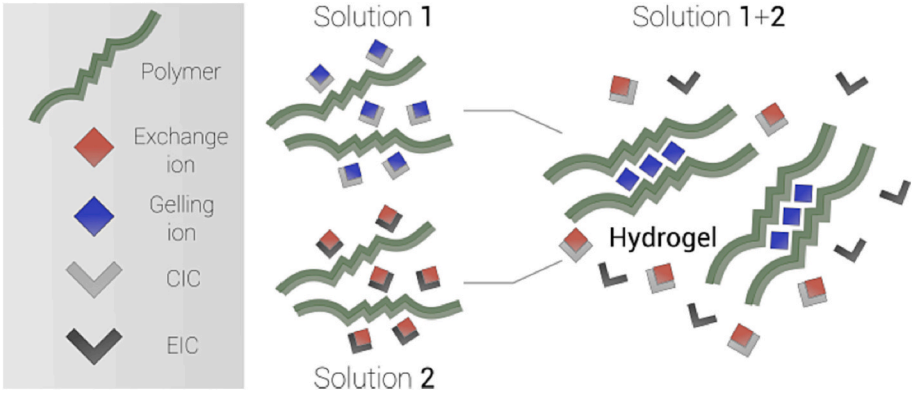

Fig. 14. Schematic illustration of the competitive ligand exchange crosslinking (CLEX) mechanism, inspired by the egg-box model often used to describe alginate gelation. A similar ionotropic polymer is present both in the aqueous crosslinking ion chelator (CIC) solution (solution 1) and the aqueous exchange ion chelator (EIC) solution (solution 2). Upon mixing the two solutions, the exchange ion displaces the gelling ion which is rendered free to crosslink the polymer.
(Reproduced with permission from (Bassett et al., 2016) (with permission).)

modulus of the network, N is the number of elastically active chains in the network (per unit volume) with a molecular weight M_c, k is the Boltzmann's constant, T is the absolute temperature, c_p is the polymer concentration.

Eq. (8) predicts a linear dependence of the shear modulus of a network from the number of elastically active polymer chains. One of the main assumptions of the rubber elasticity theory is that polymer chains composing the network are held together by point-like crosslinks (Stokke et al., 1991). Since alginate gels consist of junction zones rather than point-like cross-links, the applicability of the rubber elasticity for alginate gels has been questioned. Segeren and co-workers found, in the case of calcium limited hydrogels, an increase of the storage modulus with increasing temperature, which is an indication of the rubberlike behavior of the network. At variance, Andresen and Smidsrød, using saturated calcium alginate hydrogels, reported a decrease in the elastic modulus upon increasing the temperature (Andresen & Smidsrød, 1977). Moe and co-workers confirmed a change from an entropic elasticity (rubber-like) for calcium-limited alginate hydrogels to an enthalpic one for calcium saturated gels (Moe et al., 1992).

In general terms, the elastic modulus of polysaccharide hydrogels exceeds the one calculated using the rubber elasticity theory by a factor 3–10. This is taken into account by introducing a front factor, λ, in Eq. (8) (Eq. (9)) (Kavanagh & Ross-Murphy, 1998):

$$G = \lambda NKT \tag{9}$$

For alginate chains with approx. 300–500 repeating units (with a Gaussian distribution), the front factor λ approaches 1 for low cross-linked hydrogels, while a value up to 8 or 10 can be expected for highly cross-linked network or for alginate chains with approx. 75 repeating units (non-Gaussian behavior) (Moe et al., 1993). In line with these results, for saturated calcium alginate gels from G-rich samples a front factor as high as 14 has been estimated (Turco et al., 2011).

Alginate hydrogels in Ca^{2+}-limited conditions show a pronounced dependence of the mechanical properties from the molecular weight, with the Young's modulus becoming independent from Mw above 300,000. This was correlated with the presence of non-elastically active chains (loose ends) which do not contribute to the mechanical resistance of the gel network (Draget et al., 1993, 2005). The increase in Ca^{2+} concentration led to a quasi-linear increase in the mechanical properties of unsaturated alginate hydrogels with $F_G = 0.48$ and to a positive curvature with a higher content of guluronic acid ($F_G = 0.69$) (Draget et al., 1993). Similarly, a steady increase in the Young's modulus was seen in the $CaCO_3$ range from 10 mM to 22.5 mM, followed by a more marked increase for higher concentrations of calcium carbonate (up to 45 mM) (Fernández Farrés & Norton, 2014).

Generally, homogeneous hydrogels are prepared in calcium limited conditions. However, calcium saturated homogeneous hydrogels can be prepared using a combined approach. In a first step, a homogeneous hydrogels are formed in calcium limited conditions using $CaCO_3$ and GDL. This is then dialyzed, in a second step, against a solution of divalent cross-linking ion containing NaCl. Overall, highly homogeneous gels are obtained not only with Ca^{2+}, but also with Ba^{2+} and Sr^{2+} (Mørch et al., 2006, 2007). This approach was used to evaluate the effect of polymer concentration (C_p) on shear modulus and an approximately linear dependence was found ($G \propto C_p^{0.97}$) (Turco et al., 2011). This is in good agreement with the results by Mooney and co-workers in calcium limited conditions (Kong et al., 2002). At variance, the dependence of the Young's modulus from alginate concentration was estimated on calcium alginate gels obtained by direct dialysis of the polysaccharide against a quite high concentration of cross-linking ion showing $E \propto C_p^2$ (Smidsrød & Haug, 1972).

While it is generally accepted that the mechanical performance of saturated Ca-alginate gels is independent on the molecular weight, provided that $\overline{DP}_w \geq 400$ (Smidsrød & Haug, 1972), the effect of alginate composition has long been debated. Smidsrød and Haug found in 1972 a sigmoidal increase in the stiffness with the fraction of guluronic acid for saturated alginate hydrogels prepared by direct dialysis (Fig. 15) (Smidsrød & Haug, 1972).

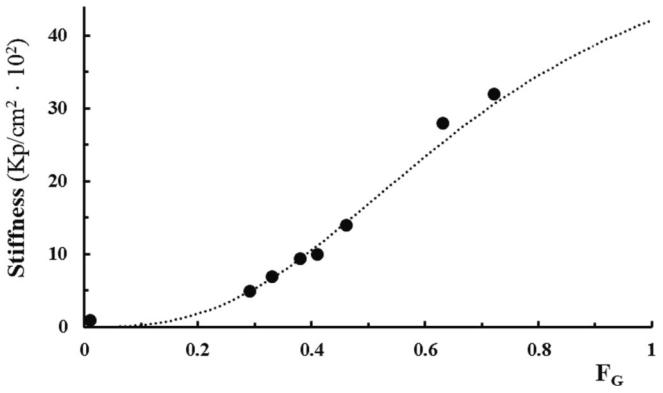

Fig. 15. Stiffness as a function of the fraction of G residues for dialyzed calcium alginate gels.
(Re-drawn from reference (Smidsrød & Haug, 1972).)

For hydrogels formed by internal gelation, Moresi and Bruno found the following power-law: $E \propto N(G/M)^{1.4}$ (Moresi & Bruno, 2007), where N(G/M) is the ratio between G and M residues in the alginate chain.

The availability of epimerases for the modification of the block composition in alginate opened up new opportunities for understanding the effect on mechanical properties. In general terms, the epimerization of natural samples, with the introduction of G residues, increases the Young's modulus of saturated hydrogels. It is also interesting to note that the highest increase was recorded when using AlgE4 epimerase which converts M-blocks in alternating sequences (MG) (Fig. 16) (Mørch et al., 2008). This effect was first attributed to a less extended elastic segment, and the correlated shorter relaxation time, upon exchanging M-blocks in MG-block (Draget et al., 2000). However, the formation of additional junctions involving MG-blocks, either GG/MG or MG/MG, could also explain this result (Donati et al., 2005).

The increase of alternating sequences in natural alginates increases the work at break per mole of junction, as well as the syneresis (Donati, Mørch, et al., 2009). The average length of the G-blocks, $\overline{N}_{G>1}$, influence the mechanical properties of Ca^{2+}-hydrogels from natural alginates. The increase of $\overline{N}_{G>1}$ from approximately 4 to 15 showed a substantial increase in the Young's modulus in natural alginate (Skjåk-Bræk et al., 1986).

The increase in $\overline{N}_{G>1}$ through epimerization with G-blocks forming epimerases led to a general increase in the mechanical properties of the calcium alginate hydrogel, although a lack of correlation with parent

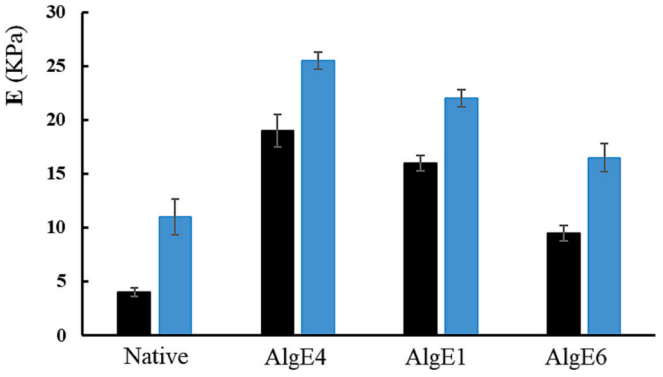

Fig. 16. Young's modulus of calcium-saturated alginate gels from *D. potatorum* (black) and L. *hyperborea* leaf (blue), native and epimerized with AlgE4, AlgE1 and AlgE6, respectively.
(Redrawn from reference (Mørch et al., 2008) (with permission).)

natural alginates was noticed (Skjåk-Bræk et al., 1986).

Hydrogels produced from epimerized mannuronan attracted particular attention. Different epimerases (AlgE) introduce G residues in G-blocks and/or MG-blocks with limited chain degradation. This powerful approach allows, in principle, to prepare hydrogels tuning the mechanical properties, syneresis and porosity (Mørch et al., 2007). The use of these engineered alginate samples proved, for the first time, that hydrogels can be obtained from polyalternating chains devoid of G-blocks, characterized by low Young's modulus and a very high elasticity (Donati et al., 2005; Mørch et al., 2007).

The introduction of G-blocks in the polyalternating sample, besides increasing the young's modulus, decreases the elasticity of the alginate hydrogel. However, it is interesting to note that the epimerized samples show a higher elasticity than calcium-hydrogels from natural alginate with the same F_G (Fig. 17). This effect was directly correlated with the presence of long MG-sequences which act as reels within the three-dimensional network (Donati, Mørch, et al., 2009).

The use of tailor-made alginate samples allowed exploring further the role of the length of G-blocks on mechanical properties of alginate hydrogels. A comparison between a natural alginate (from. *L. hyperborea)* and an epimerized alginate sample with the same F_G revealed that the Young's modulus was much higher in the former case than in the latter. This was traced back to the different length of the G-blocks between the two samples that, thanks to analytical tools developed, was determined as distribution and not just as NMR average. In the case of *L. hyperborea*, very long G-blocks are present (DP > 100), while in the epimerized alginate with the same F_G, the G-blocks are shorter (DP 30–50) (Aarstad et al., 2013).

The possibility of preparing homogeneous saturated alginate hydrogels allows measuring the effects of different ions on their mechanical properties (Mørch et al., 2006). In the case of high-G alginates, with respect to Ca^{2+}-hydrogels prepared in aqueous 50 mM of $CaCl_2$, the addition of as little as 1 mM of $BaCl_2$ increases the Young's modulus of approx. 80 %. The use of an aqueous cross-linking solution of 10 mM and 20 mM $BaCl_2$, respectively, increases further the mechanical performance of the hydrogel. Finally, also the use of aqueous 50 mM $SrCl_2$ leads to a net increase in the mechanical properties of alginate hydrogels with respect to aqueous 50 mM $CaCl_2$. This is in line with the reported ion binding affinity for high-G alginates: $Ba^{2+} > Sr^{2+} > Ca^{2+}$. This was not the case for high-M alginates, where the addition of $BaCl_2$ 1 mM does not lead to marked variation in Young's modulus, while the use of Sr^{2+} is detrimental. Only the use of aqueous $BaCl_2$ at 10 mM or 20 mM brings about an increase in the Young's modulus with respect to aqueous $CaCl_2$ 50 mM (Fig. 18).

In summary, the strength of alginate hydrogels is improved by

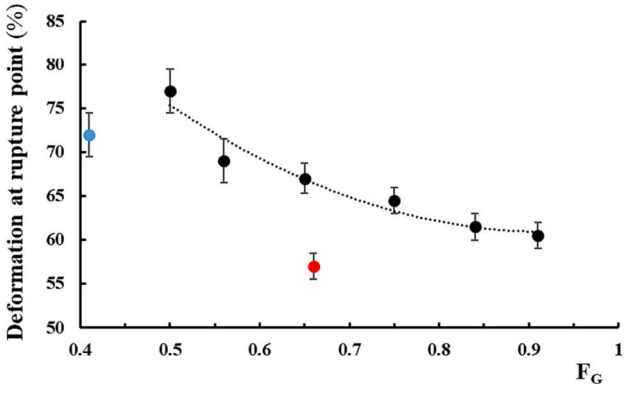

Fig. 17. Elasticity, measured as deformation at rupture point, of saturated calcium-alginate hydrogels of AlgE1-epimerized polyMG samples with different G contents (F_G) and of native samples from L. *hyperborea* (red) and *M. pyrifera* (blue).
(Redrawn from reference (Mørch et al., 2007) (with permission).)

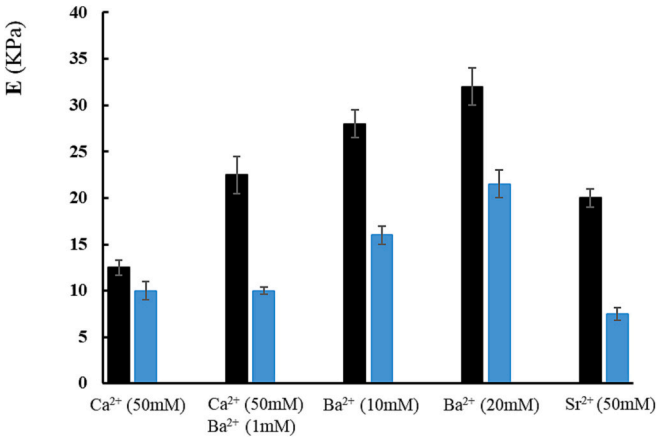

Fig. 18. Young's modulus (E) for homogeneous hydrogels obtained with different divalent ions for high-G alginate from L. *hyperborea* (black) and for high-M alginate from *M. pyrifera* (blue).
(Redrawn from reference (Mørch et al., 2006) (with permission).)

increasing the amount of G residues, the amount of divalent cations in solution and the use of strong binding metal ions, such as Ba^{2+}. However, the contribution of the different sequences to ion binding and chain flexibility, as well as their ion selectivity, suggest caution in drawing general conclusions on such subject.

9.6. Porosity, swelling and stability

Electron microscopy (TEM) determined the dimension and distribution of pores in alginate hydrogels in the range from 5 to 200 nm, with the higher fraction at around 25 nm (Andresen et al., 1977). Analyses of TEM images on saturated homogeneous calcium alginate gels showed a slightly narrower distribution, up to 100 nm, with the maximum probability in the pore dimension at around 9 nm (Turco et al., 2011). Alternatively, the average dimension of the pores, $\overline{\delta}$, was determined by measuring the average transversal relaxation time of water, $\overline{T}_2$ (Eq. (10)):

$$\overline{T}_2 = k\overline{\delta} \tag{10}$$

where k is a constant which depends on the geometry and inner surface properties (Britton et al., 2004).In the case of a Ca^{2+}-alginate gel, the highest probability in $\overline{\delta}$ corresponded to 6–7 nm, while an additional probability peak was found at around 14 nm (Turco et al., 2011). Another estimation of the porosity of Ca^{2+}-alginate hydrogels came from the diffusion of dextran and the calculation of the volume probability density function points to a pore size of about 16 nm (Rolland et al., 2014). A slightly larger mesh size (maximum probability of pore size of about 40 nm) for Ca^{2+}-alginate hydrogels is estimated by computational methods (Campbell et al., 2020).

The use of the rubber elasticity theory (Eq. (9)) allowed an estimation of the average pore size from the shear modulus, G (Eq. (11)):

$$\overline{\delta} = \sqrt[3]{\frac{6\lambda RT}{\pi N_A G}} \tag{11}$$

where N_A is the Avogadro's number. In this case, an average pore size of approx. 9.8 nm is found, with a polymer concentration dependence of $\overline{\delta} \propto c_p^{-0.32}$ (Turco et al., 2011).

Divalent cross-linking ions and alginate composition strongly influence the dimension of the pores. Interestingly enough, the use of a high-G alginate results in a more permeable hydrogel with respect to high-M alginate when Ca^{2+} is used as cross-linking ion (Mørch et al., 2006). This effect could be linked to the role of the alternating sequences, which are present in a higher fraction in high-M alginates, that by favoring the

clustering of junctions into bundles or binding of Ca^{2+} cause a collapse in the network.

Engineered alginates produced with long MG stretches using AlgE4 support this conclusion, showing a very low permeability. Indeed, upon increasing the amount of G blocks with AlgE1, at the cost of reducing the alternating sequences, the permeability of the hydrogel increases (Mørch et al., 2007).

The role of the different divalent ions on hydrogel permeability strictly depends on their affinity for the alginate sequences. As an example, the use of Ba^{2+} as cross-linking ion decreases the permeability of alginate by approx. 70 % when the concentration of the divalent ions equals 20 mM. At variance, when high-M alginate is considered, the replacement of Ca^{2+} with Ba^{2+} actually slightly increases the permeability of the hydrogel. Finally, the role of Sr^{2+} on the permeability is negligible for both high-G and high-M alginates (Mørch et al., 2006).

The dimension of a polyelectrolyte hydrogel in a solvent is determined from the balancing of the elastic force (π^{elast}), which acts against volume expansions, and of the osmotic pressure (π^{osm}), which acts increasing the dimension of the network. Variations in the number of junctions, i.e. in the elastically active chains, in alginate network affect the overall volume of the hydrogel. The treatment of Ca^{2+}-alginate hydrogel with chelating agents such as EDTA, lactate and citrate removes the cross-linking ion from the junctions reducing their number, as well as the number of elastically active chains. An increase in the volume of the hydrogel restores the equilibrium. If the concentration of the chelating agent is high enough, a complete dissolution of the Ca^{2+}-alginate hydrogel takes place. An excess of Na^{+} as competing ion causes a similar effect. Despite the higher affinity of alginate, and in particular of G blocks, towards Ca^{2+} with respect to Na^{+}, the use of high amounts of the latter will displace the cross-linking ions for the junctions. An increase in the volume (swelling) of the gel then occurs.

The dimensional stability of Ca^{2+}-alginate hydrogels towards the competing Na^{+} ions for natural alginates depends on the length of the G-blocks and on the overall F_G content. Ca^{2+}-alginate gels from L. *hyperborea* ($\overline{N}_{G>1} = 14.5$) show lower swelling, i.e. higher dimensional stability, than hydrogels from *M. pyrifera* ($\overline{N}_{G>1} = 4.2$), which in turn is more stable than hydrogels from *A. nodosum* ($\overline{N}_{G>1} = 2.0$) (Fig. 19a) (Donati, Mørch, et al., 2009). A non-monotonic dependence of the swelling from the fraction of G residues, F_G, was reported for engineered alginates (Fig. 19b) (Mørch et al., 2007). In this sense it should be underlined that the elongation of MG block brings about a general increase in stability of the natural and epimerized alginates hydrogels (Donati, Mørch, et al., 2009; Strand, Mørch, Syvertsen, et al., 2003). The ion affinity by different alginate sequences has a strong effect on the dimensional stability of the alginate hydrogels. The replacement of Ca^{2+} with Ba^{2+}, due to the higher number of junctions and an increased resistance to the displacement by Na^{+} ions, leads to a marked increase in dimensional stability of the network (Fig. 19c) (Mørch et al., 2006).

10. Cation exchange: specificity of alginates for divalent cations

As mentioned above, the reactivity and gel formation with Ca^{2+} remains the major use of alginates. Except for Mg^{2+} (see below) other alkali earth metals interact even more avidly with alginates. In the 1960s it was observed that Sr/Ca ratio in brown seaweeds could be 20 times higher than that of the surrounding sea water (Haug & Smidsrød, 1968). This could be explained by higher selectivity of the alginate for Sr compared to Ca (Haug & Smidsrød, 1967).

Numerous studies showed that the selectivity for Ca^{2+} was a property of the G-blocks. In this context the selectivity is expressed relative to

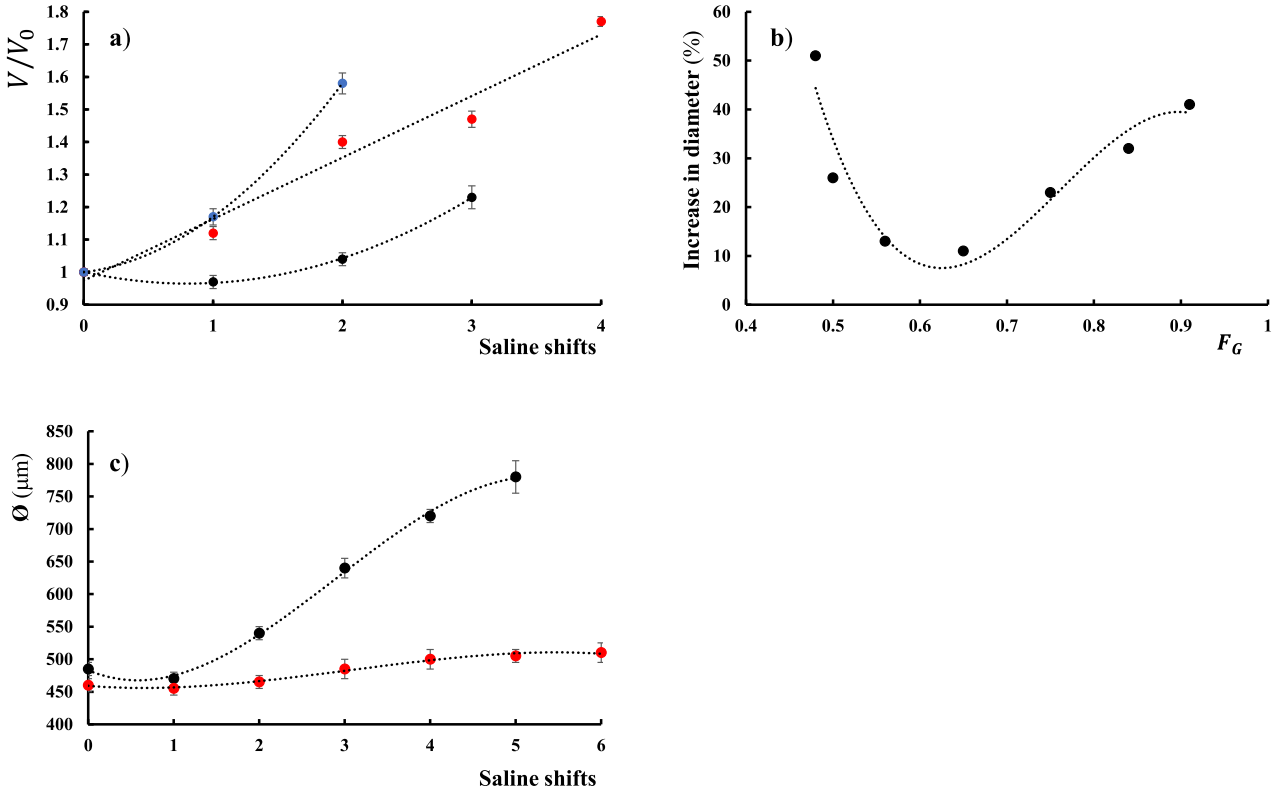

Fig. 19. **a**) Relative volume variation (V/V_0) of homogeneous saturated calcium-alginate hydrogels from L. *hyperborea* (black), *M. pyrifera* (red), and *A. nodosum* (blue) upon treatment with saline solution for different shifts. V refers to the volume of the hydrogel at a specific saline shift while V_0 is the initial volume of the hydrogel. Redrawn from reference (Donati, Mørch, et al., 2009). **b**) Increase in diameter of alginate beads for epimerized calcium alginate hydrogels after 7 saline (NaCl) solution shifts as a function of the fraction of G residues (F_G). Redrawn from reference (Mørch et al., 2007) (with permission) **c**) Diameter of alginate beads from L. *hyperborea* reticulated with Ca^{2+} (black) and Ba^{2+} (red), respectively, upon treatment with saline solution for different shifts. Redrawn from reference (Mørch et al., 2006) (with permission).

a second cation since cation binding is an exchange process. Since Mg^{2+} has the same charge as other alkali earth metals and the fact that Mg-alginates remain water-soluble, Mg^{2+} has frequently been used as a reference ion in cation exchange studies according to (Eq. (12)):

$$AlgMg + Me^{2+} = AlgMe + Mg^{2+} \quad (12)$$

The corresponding selectivity coefficient K_{Mg}^{Me} is defined as the molar ratio of bound (subscript b) cations ($n_{Me,b}/n_{Mg,b}$) relative to the corresponding ratio in solution (subscript l) (Eq. (13)):

$$K_{Mg}^{Me} = \frac{n_{Me,b}}{n_{Mg,b}} \Big/ \frac{[Me_l]}{[Mg_l]} = \frac{X_{Me,b}}{X_{Mg,b}} \frac{[Mg_l]}{[Me_l]} \quad (13)$$

Here, X refers to the mole fraction of bound cations. Most data from this period were taken for conditions providing X_{Me} close to 0.5, using equilibrium dialysis as the main experimental method. It was soon found that the selectivity for Ca^{2+} was very high and that it was primarily associated with the G-blocks and the insoluble material associated with Ca-binding. Further, the selectivity depended not only the alginate type, but also on the amount of bound Ca (expressed by X_{Ca}) (Fig. 20a).

The Ca-selectivities for both M-rich and MG-rich alginates are low and little dependent on the amount of bound calcium, whereas G-rich alginates have rapidly increasing values leading to a maximum at $X_{Ca} = 0.4$ whereafter it decreases again. Another key feature of Ca-binding is hysteresis: After first saturating the alginate with calcium ($X_{Ca} = 1$) and then introducing gradually increasing amounts of magnesium the Ca-selectivity rose above the previous maximum. This 'memory' effect has been interpreted as Ca-induced chain dimerization and "egg-box" formation.

The selectivity for Sr and Ba followed the pattern observed for Ca but is progressively shifted to higher selectivities and maxima at lower X_{Me} values (Fig. 20b). The stronger binding of these cations has been used to improve material properties of Ca-alginate gels by including small amounts of barium (Mørch et al., 2006). Priming with Sr has also recently been used to design alginate-based systems for Sr-removal from oil fields (Liu et al., 2021).

It may be noted that few quantitative data (selectivity coefficients) exist for situations where the degree of Ca^{2+} saturation is low. Likewise, equilibrium data for Ca-alginate (gels, fibers, film etc.) for example in physiological saline, hardly exist. On the other hand, numerous studies describe the dynamics of Ca^{2+}- Na^{+} exchange under physiological conditions. Ca^{2+}-alginate beads, which are highly relevant for micro-encapsulation of live cells, gradually swell and disintegrate in physiological saline (1.2 mM Ca^{2+}, 150 mM Na^{+}) and will for long term stability need additional stabilizing factors. Of these, 'doping' with a small proportion of Ba^{2+} (Ba/Ca = 1/50) takes advantage of the stronger binding of Ba^{2+} to alginate and provides more stable gels (Mørch et al., 2006, 2012).

11. Alginate based diblock polysaccharides and nanoparticle formation by self-assembly

Alginate chains can be selectively substituted at the reducing end by a second chain using dioxyamine or dihydrazide linkers forming anti-parallel diblock polysaccharides (Solberg et al., 2021, 2023) (Fig. 21). The dihydrazide and dioxyamine chemistry have been described in detail elsewhere (Solberg et al., 2022).

The system balances the strong and chain length dependent affinity of G-blocks for Ca^{2+} ions (Kohn & Larsen, 1972) leading to initial chain dimerization and subsequent lateral growth with the outer dextran chains. The latter prevents indefinite growth by gradually saturating the nanoparticle surface due to excluded volume effects. Therefore, only certain combinations of chain lengths give well-defined nanoparticles, although systematic studies of the chain length dependency and selectivity of Ca^{2+} have not yet been carried out. The system is related to the self-assembly of synthetic block copolymers although the strong and specific Ca^{2+}-G-block interaction seems unique for the system.

12. Radionuclides and alginate

A relatively new development in medicine and theranostics is targeted radiation therapy, where radiopharmaceuticals are delivered specifically to tumour lesions for therapeutic purposes. This involves α, β or γ-emitting isotopes of cations (radionuclides), some of which have high affinities to alginates, either due to high charge or the ability to stabilize chain dimerization through the 'egg-box' model. ^{227}Ra is an α-emitter which is currently used in cancer therapy as a simple salt, but realizing it belongs to group 2 of the periodic table (as do Ca, Sr, Ba) high affinity to alginate is predicted. Indeed, uptake of ^{227}Ra to Ca^{2+}- and Sr^{2+}-alginate microbeads has been described (Frenvik et al., 2016). For other clinically relevant α-emitters (actinium-225, astatine-211, bismuth-212, bismuth-213, lead-212, terbium-149, thorium-227) (Eychenne et al., 2021) the interaction with alginates has apparently not been studied in any detail although several patents or patent applications exist. The area should be attractive due to the favorable biomedical

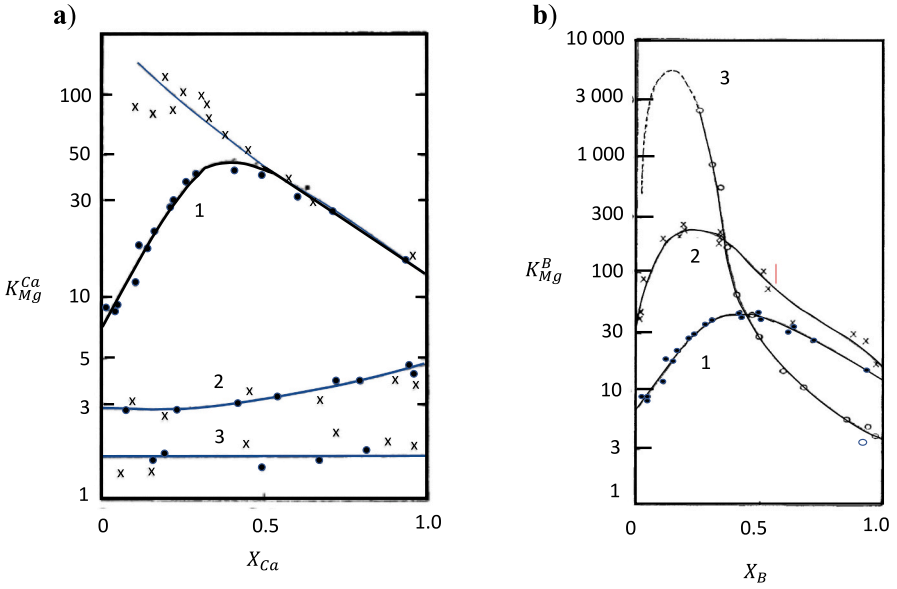

Fig. 20. a) The selectivity coefficient K_{Mg}^{Ca} for alginate fragments against the equivalent fraction X_{Ca} of calcium bound to the polyelectrolyte. Curve 1: $F_G = 0.90$, $DP_n = 50$. Curve 2: Alternating fragment, $F_G = 0.38$, $DP_n = 20$. Curve 3: Fragment with $F_M = 0.90$, $DP_n = 26$. •: Dialysis against the fragments in their Na^{+} for. X: Dialysis first against 0.2 M $CaCl_2$, then against mixtures of $CaCl_2$ and $MgCl_2$. Redrawn from (Haug et al., 1967) (with permission). **b**) The selectivity coefficient K_{Mg}^{B} against X_B for different alkaline earth ions B for a fragment with $F_G = 0.90$, $DP_n = 50$. Curve 1: B = Ca. Curve 2: B = Sr. Curve 3: B = Ba. Redrawn from (Smidsrød, 1974) (with permission).

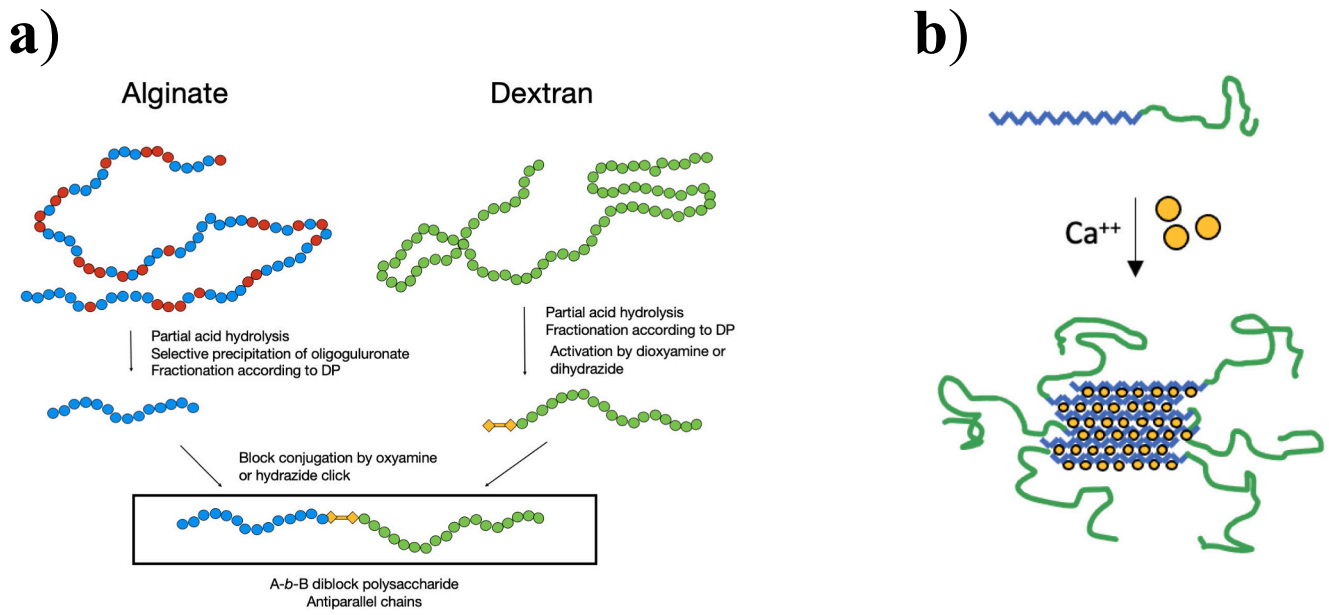

Fig. 21. **a**) Preparation of G_m-b-Dex_n diblock polysaccharides. G-blocks (oligoguluronate blocks) are obtained from a parent G-rich alginate by partial acid hydrolysis and fractional precipitation. Dextran blocks are obtained by partial acid hydrolysis. Different chain lengths (m,n) are obtained via SEC fractionation. The dextran block is terminally substituted at the reducing end by a dioxyamine (PDHA) or a dihydrazide (ADH) before coupling to the reducing end of the G-block. **b**) Ca-induced self-assembly of G_m-b-Dex_n diblock polysaccharides into core-corona nanoparticles with Ca-alginate as the core and the Ca-insensitive dextran forming the corona.

properties of alginates.

Declaration of competing interest

The authors declare that they have no known competing financial interests or personal relationships that could have appeared to influence the work reported in this paper.

Data availability

No data was used for the research described in the article.

References

Aarstad, O., Strand, B. L., Klepp-Andersen, L. M., & Skjåk-Bræk, G. (2013). Analysis of G-block distributions and their impact on gel properties of in vitro epimerized mannuronan. *Biomacromolecules, 14*(10), 3409–3416. https://doi.org/10.1021/bm400658k

Andresen, I.-L., Skipnes, O., Smidsrød, O., Ostgaard, K., & Hemmer, P. C. (1977). Some biological functions of matrix components in benthic algae in relation to their chemistry and the composition of seawater. In , *Vol. 48. Cellulose chemistry and technology* (pp. 24–361). AMERICAN CHEMICAL SOCIETY. https://doi.org/10.1021/bk-1977-0048.ch024.

Andresen, I.-L., & Smidsrød, O. (1977). Temperature dependence of the elastic properties of alginate gels. *Carbohydrate Research, 58*(2), 271–279. https://doi.org/10.1016/S0008-6215(00)84354-2

Bassett, D. C., Håti, A. G., Melø, T. B., Stokke, B. T., & Sikorski, P. (2016). Competitive ligand exchange of crosslinking ions for ionotropic hydrogel formation. *Journal of Materials Chemistry B, 4*(37), 6175–6182. https://doi.org/10.1039/C6TB01812B

Bi, D., Yang, X., Yao, L., Hu, Z., Li, H., Xu, X., & Lu, J. (2022). Potential food and nutraceutical applications of alginate: A review. *Marine Drugs, 20*(9). https://doi.org/10.3390/md20090564

Bochenek, M. A., Veiseh, O., Vegas, A. J., McGarrigle, J. J., Qi, M., Marchese, E., … Oberholzer, J. (2018). Alginate encapsulation as long-term immune protection of allogeneic pancreatic islet cells transplanted into the omental bursa of macaques. *Nature Biomedical Engineering, 2*(11), 810–821. https://doi.org/10.1038/s41551-018-0275-1

Borgogna, M., Skjåk-Bræk, G., Paoletti, S., & Donati, I. (2013). On the initial binding of alginate by calcium ions. The tilted egg-box hypothesis. *Journal of Physical Chemistry B, 117*(24), 7277–7282. https://doi.org/10.1021/jp4030766

Borukhov, I., Lee, K.-C., Bruinsma, R. F., Gelbart, W. M., Liu, A. J., & Stevens, M. J. (2002). Association of two semiflexible polyelectrolytes by interchain linkers: Theory and simulations. *The Journal of Chemical Physics, 117*(1), 462–480. https://doi.org/10.1063/1.1481382

Bowman, K. A., Aarstad, O. A., Nakamura, M., Stokke, B. T., Skjåk-Bræk, G., & Round, A. N. (2016). Single molecule investigation of the onset and minimum size of the calcium-mediated junction zone in alginate. *Carbohydrate Polymers, 148*, 52–60. https://doi.org/10.1016/j.carbpol.2016.04.043

Braccini, I., & Pérez, S. (2001). Molecular basis of Ca2+-induced gelation in alginates and pectins: The egg-box model revisited. *Biomacromolecules, 2*(4), 1089–1096. https://doi.org/10.1021/bm010008g

Britton, M. M., Graham, R. G., & Packer, K. J. (2004). NMR relaxation and pulsed field gradient study of alginate bead porous media. *Journal of Magnetic Resonance, 169*(2), 203–214. https://doi.org/10.1016/j.jmr.2004.04.016

Campbell, K. T., Wysoczynski, K., Hadley, D. J., & Silva, E. A. (2020). Computational-based design of hydrogels with predictable mesh properties. *ACS Biomaterials Science & Engineering, 6*(1), 308–319. https://doi.org/10.1021/acsbiomaterials.9b01520

Cao, Y., Cong, H., Yu, B., & Shen, Y. (2023). A review on the synthesis and development of alginate hydrogels for wound therapy. *Journal of Materials Chemistry B, 11*(13), 2801–2829. https://doi.org/10.1039/D2TB02808E

Chaudhuri, O., Gu, L., Darnell, M., Klumpers, D., Bencherif, S. A., Weaver, J. C., … Mooney, D. J. (2015). Substrate stress relaxation regulates cell spreading. *Nature Communications, 6*(1), 6365. https://doi.org/10.1038/ncomms7365

Christensen, B. E., Skjåk-Bræk, G., & Smidsrød, O. (2007). Comment on "conformational changes and aggregation of alginic acid as determined by fluorescence correlation spectroscopy". *Biomacromolecules, 8*(10), 3279. https://doi.org/10.1021/bm078004k

de Vos, P., Faas, M. M., Strand, B., & Calafiore, R. (2006). Alginate-based microcapsules for immunoisolation of pancreatic islets. *Biomaterials, 27*(32), 5603–5617. https://doi.org/10.1016/j.biomaterials.2006.07.010

Decho, A. W. (1999). Imaging an alginate polymer gel matrix using atomic force microscopy. *Carbohydrate Research, 315*(3), 330–333. https://doi.org/10.1016/S0008-6215(99)00006-3

Dodero, A., Alberti, S., Gaggero, G., Ferretti, M., Botter, R., Vicini, S., & Castellano, M. (2021). An up-to-date review on alginate nanoparticles and nanofibers for biomedical and pharmaceutical applications. *Advanced Materials Interfaces, 8*(22), 2100809. https://doi.org/10.1002/admi.202100809

Donati, I., Asaro, F., & Paoletti, S. (2009). Experimental evidence of counterion affinity in alginates: The case of nongelling ion Mg2+. *Journal of Physical Chemistry B, 113*(39), 12877–12886. https://doi.org/10.1021/jp902912m

Donati, I., Cesàro, A., & Paoletti, S. (2006). Specific interactions versus counterion condensation. 1. Nongelling ions/polyuronate systems. *Biomacromolecules, 7*(1), 281–287. https://doi.org/10.1021/bm050646p

Donati, I., Holtan, S., Mørch, Y. A., Borgogna, M., Dentini, M., & Skjåk-Bræk, G. (2005). New hypothesis on the role of alternating sequences in calcium–alginate gels. *Biomacromolecules, 6*(2), 1031–1040. https://doi.org/10.1021/bm049306e

Donati, I., Mørch, Y. A., Strand, B. L., Skjåk-Braek, G., & Paoletti, S. (2009). Effect of elongation of alternating sequences on swelling behavior and large deformation properties of natural alginate gels. *Journal of Physical Chemistry B, 113*(39), 12916–12922. https://doi.org/10.1021/jp905488u

Donati, I., & Paoletti, S. (2009). In B. H. A. Rehm (Ed.), *Material properties of alginates - alginates: Biology and applications* (pp. 1–53). Berlin Heidelberg: Springer. https://doi.org/10.1007/978-3-540-92679-5_1.

Draget, K. I., Moe, S. T., Skjåk-Bræk, G., Smidsrød, O., Phillips, A. M., & Williams, G. O. (2006). Alginates. In P. A. Stephen (Ed.), *Food polysaccharides and their applications* (pp. 289–334). CRC Press.

Draget, K. I., Østgaard, K., & Smidsrød, O. (1990). Homogeneous alginate gels: A technical approach. *Carbohydrate Polymers, 14*(2), 159–178. https://doi.org/10.1016/0144-8617(90)90028-Q

Draget, K. I., Simensen, M. K., Onsøyen, E., & Smidsrød, O. (1993). Gel strength of Ca-limited alginate gels made in situ. *Hydrobiologia, 260*(1), 563–565. https://doi.org/10.1007/BF00049071

Draget, K. I., Skjåk Bræk, G., & Smidsrød, O. (1994). Alginic acid gels: The effect of alginate chemical composition and molecular weight. *Carbohydrate Polymers, 25*(1), 31–38. https://doi.org/10.1016/0144-8617(94)90159-7

Draget, K. I., Skjåk-Bræk, G., Christensen, B. E., Gåserød, O., & Smidsrød, O. (1996). Swelling and partial solubilization of alginic acid gel beads in acidic buffer. *Carbohydrate Polymers, 29*(3), 209–215. https://doi.org/10.1016/0144-8617(96)00029-X

Draget, K. I., Smidsrød, O., & Skjåk-Bræk, G. (2005). Alginates from algae. *Biopolymers Online*. https://doi.org/10.1002/3527600035.bpol6008

Draget, K. I., Stokke, B. T., Yuguchi, Y., Urakawa, H., & Kajiwara, K. (2003). Small-angle X-ray scattering and rheological characterization of alginate gels. 3. alginic acid gels. *Biomacromolecules, 4*(6), 1661–1668. https://doi.org/10.1021/bm034105g

Draget, K. I., Strand, B., Hartmann, M., Valla, S., Smidsrød, O., & Skjåk-Bræk, G. (2000). Ionic and acid gel formation of epimerised alginates; the effect of AlgE4. *International Journal of Biological Macromolecules, 27*(2), 117–122. https://doi.org/10.1016/S0141-8130(00)00115-X

Eychenne, R., Chérel, M., Haddad, F., Guérard, F., & Gestin, J.-F. (2021). Overview of the most promising radionuclides for targeted alpha therapy: The "hopeful eight". *Pharmaceutics, 13*(6). https://doi.org/10.3390/pharmaceutics13060906

Fang, Y., Al-Assaf, S., Phillips, G. O., Nishinari, K., Funami, T., Williams, P. A., & Li, L. (2007). Multiple steps and critical behaviors of the binding of calcium to alginate. *The Journal of Physical Chemistry B, 111*(10), 2456–2462. https://doi.org/10.1021/jp0689870

Fernández Farrés, I., & Norton, I. T. (2014). Formation kinetics and rheology of alginate fluid gels produced by in-situ calcium release. *Food Hydrocolloids, 40*, 76–84. https://doi.org/10.1016/j.foodhyd.2014.02.005

Flory, P. J. (1953). *Principles of polymer chemistry. 1953*. Ithaca: Cornell University Press. https://search.library.wisc.edu/catalog/999474843502121.

Frenvik, J. O., Kristensen, S., & Ryan, O. B. (2016). Development of separation technology for the removal of radium-223 from decayed thorium-227 in drug formulations. Material screening and method development. *Drug Development and Industrial Pharmacy, 42*(8), 1215–1224. https://doi.org/10.3109/03639045.2015.1118494

Gimmestad, M., Sletta, H., Ertesvåg, H., Bakkevig, K., Jain, S., Suh, S., … Valla, S. (2003). The Pseudomonas fluorescens AlgG protein, but not its mannuronan C-5-epimerase activity, is needed for alginate polymer formation. *Journal of Bacteriology, 185*(12), 3515–3523. https://doi.org/10.1128/JB.185.12.3515-3523.2003

Grant, G. T., Morris, E. R., Rees, D. A., Smith, P. J. C., & Thom, D. (1973). Biological interactions between polysaccharides and divalent cations: The egg-box model. *FEBS Letters, 32*(1), 195–198. https://doi.org/10.1016/0014-5793(73)80770-7

Grasdalen, H., & Kvam, B. J. (1986). Sodium-23 NMR in aqueous solutions of sodium polyuronates. Counterion binding and conformational conditions. *Macromolecules, 19*(7), 1913–1920. https://doi.org/10.1021/ma00161a022

Håti, A. G., Bassett, D. C., Ribe, J. M., Sikorski, P., Weitz, D. A., & Stokke, B. T. (2016). Versatile, cell and chip friendly method to gel alginate in microfluidic devices. *Lab on a Chip, 16*(19), 3718–3727. https://doi.org/10.1039/C6LC00769D

Haug, A. (1964). *Composition and properties of alginates*.

Haug, A., Larsen, B., & Smidsrød, O. (1967). Studies on the sequence of uronic acid residues in alginic acid. *Acta Chemica Scandinavica, 21*, 691–704.

Haug, A., & Smidsrød, O. (1967). Strontium–calcium selectivity of alginates. *Nature, 215*(5102), 757. https://doi.org/10.1038/215757a0

Haug, A., & Smidsrød, O. (1968). The solubility of polysaccharides in salt solutions. *Chemical Society Special Publication, 23*, 273–280.

Haug, A., & Smidsrød, O. (1970). Selectivity of some anionic polymers for divalent metal ions. *Acta Chemica Scandinavica, 24*, 843–854.

Heinemann, M., Meinberg, H., Büchs, J., Koß, H.-J., & Ansorge-Schumacher, M. B. (2005). Method for quantitative determination of spatial polymer distribution in alginate beads using Raman spectroscopy. *Applied Spectroscopy, 59*(3), 280–285. https://doi.org/10.1366/0003702053585363

Hernández-González, A. C., Téllez-Jurado, L., & Rodríguez-Lorenzo, L. M. (2020). Alginate hydrogels for bone tissue engineering, from injectables to bioprinting: A review. *Carbohydrate Polymers, 229*, Article 115514. https://doi.org/10.1016/j.carbpol.2019.115514

Hu, C., Lu, W., Mata, A., Nishinari, K., & Fang, Y. (2021). Ions-induced gelation of alginate: Mechanisms and applications. *International Journal of Biological Macromolecules, 177*, 578–588. https://doi.org/10.1016/j.ijbiomac.2021.02.086

Kashiwagi, Y., Norisuye, T., & Fujita, H. (1981). Triple helix of Schizophyllum commune polysaccharide in dilute solution. 4. Light scattering and viscosity in dilute aqueous sodium hydroxide. *Macromolecules, 14*(5), 1220–1225. https://doi.org/10.1021/ma50006a016

Kavanagh, G. M., & Ross-Murphy, S. B. (1998). Rheological characterisation of polymer gels. *Progress in Polymer Science, 23*(3), 533–562. https://doi.org/10.1016/S0079-6700(97)00047-6

Khorramian, B. A., & Stivala, S. S. (1982). Assessment of branching in hydrolysates of S. salivarius levan and L. mesenteroides dextran from small-angle X-ray scattering. *Carbohydrate Research, 108*(1), 1–11. https://doi.org/10.1016/S0008-6215(00)81884-4

Kohn, R. (1975). Ion binding on polyuronates - Alginate and pectin. *Pure and Applied Chemistry, 42*, 371–397.

Kohn, R., & Larsen, B. (1972). Preparation of water-soluble polyuronic acids and their calcium salts, and the determination of calcium ion activity in relation to the degree of polymerization. *Acta Chemica Scandinavica, 26*, 2455–2468.

Kong, H. J., Lee, K. Y., & Mooney, D. J. (2002). Decoupling the dependence of rheological/mechanical properties of hydrogels from solids concentration. *Polymer, 43*(23), 6239–6246. https://doi.org/10.1016/S0032-3861(02)00559-1

Kroneková, Z., Pelach, M., Mazancová, P., Uhelská, L., Treľová, D., Rázga, F., … Lacík, I. (2018). Structural changes in alginate-based microspheres exposed to in vivo environment as revealed by confocal Raman microscopy. *Scientific Reports, 8*(1), 1637. https://doi.org/10.1038/s41598-018-20022-y

Larobina, D., & Cipelletti, L. (2013). Hierarchical cross-linking in physical alginate gels: A rheological and dynamic light scattering investigation. *Soft Matter, 9*(42), 10005–10015. https://doi.org/10.1039/C3SM52006D

Lattner, D., Flemming, H.-C., & Mayer, C. (2003). 13C-NMR study of the interaction of bacterial alginate with bivalent cations. *International Journal of Biological Macromolecules, 33*(1), 81–88. https://doi.org/10.1016/S0141-8130(03)00070-9

Lee, H., Venable, R. M., MacKerell, A. D., Jr., & Pastor, R. W. (2008). Molecular dynamics studies of polyethylene oxide and polyethylene glycol: Hydrodynamic radius and shape anisotropy. *Biophysical Journal, 95*(4), 1590–1599. https://doi.org/10.1529/biophysj.108.133025

Liu, C., Yu, X., Ma, C., Guo, Y., & Deng, T. (2021). Selective recovery of strontium from oilfield water by ion-imprinted alginate microspheres modified with thioglycollic acid. *Chemical Engineering Journal, 410*, Article 128267. https://doi.org/10.1016/j.cej.2020.128267

Maki, Y., Ito, K., Hosoya, N., Yoneyama, C., Furusawa, K., Yamamoto, T., … Wakabayashi, K. (2011). Anisotropic structure of calcium-induced alginate gels by optical and small-angle X-ray scattering measurements. *Biomacromolecules, 12*(6), 2145–2152. https://doi.org/10.1021/bm200223p

Martinsen, A., Storrø, I., & Skjåk-Bræk, G. (1992). Alginate as immobilization material: III. Diffusional properties. *Biotechnology and Bioengineering, 39*(2), 186–194. https://doi.org/10.1002/bit.260390210

Moe, S. T., Draget, K. I., Skjåk-Bræk, G., & Simdsrød, O. (1992). Temperature dependence of the elastic modulus of alginate gels. *Carbohydrate Polymers, 19*(4), 279–284. https://doi.org/10.1016/0144-8617(92)90081-Z

Moe, S. T., Elgsaeter, A., Skjåk-Bræk, G., & Smidsrød, O. (1993). A new approach for estimating the crosslink density of covalently crosslinked ionic polysaccharide gels. *Carbohydrate Polymers, 20*(4), 263–268. https://doi.org/10.1016/0144-8617(93)90098-O

Mørch, Y. A., Donati, I., Strand, B. L., & Skjåk-Bræk, G. (2006). Effect of Ca2+, Ba2+, and Sr2+ on alginate microbeads. *Biomacromolecules, 7*(5), 1471–1480. https://doi.org/10.1021/bm060010d

Mørch, Y. A., Donati, I., Strand, B. L., & Skjåk-Bræk, G. (2007). Molecular engineering as an approach to design new functional properties of alginate. *Biomacromolecules, 8*(9), 2809–2814. https://doi.org/10.1021/bm700502b

Mørch, Y. A., Holtan, S., Donati, I., Strand, B. L., & Skjåk-Bræk, G. (2008). Mechanical properties of C-5 epimerized alginates. *Biomacromolecules, 9*(9), 2360–2368. https://doi.org/10.1021/bm8003572

Mørch, Y. A., Qi, M., Gundersen, P. O. M., Formo, K., Lacik, I., Skjåk-Bræk, G., … Strand, B. L. (2012). Binding and leakage of barium in alginate microbeads. *Journal of Biomedical Materials Research Part A, 100A*(11), 2939–2947. https://doi.org/10.1002/jbm.a.34237

Moresi, M., & Bruno, M. (2007). Characterisation of alginate gels using quasi-static and dynamic methods. *Journal of Food Engineering, 82*(3), 298–309. https://doi.org/10.1016/j.jfoodeng.2007.02.040

Neves, M. I., Moroni, L., & Barrias, C. C. (2020). Modulating alginate hydrogels for improved biological performance as cellular 3D microenvironments. *Frontiers in Bioengineering and Biotechnology, 8*. https://www.frontiersin.org/articles/10.3389/fbioe.2020.00665.

Odijk, T. (1977). Polyelectrolytes near the rod limit. *Journal of Polymer Science Polymer Physics Edition, 15*(3), 477–483. https://doi.org/10.1002/pol.1977.180150307

Paoletti, S., & Donati, I. (2022). Comparative insights into the fundamental steps underlying gelation of plant and algal ionic polysaccharides: Pectate and alginate. *Gels, 8*(12). https://doi.org/10.3390/gels8120784

Paoletti, S., Smidsrod, O., & Grasdalen, H. (1984). Thermodynamic stability of the ordered conformations of carrageenan polyelectrolytes. *Biopolymers, 23*(9), 1771–1794. https://doi.org/10.1002/bip.360230911

Perić-Hassler, L., & Hünenberger, P. H. (2010). Interaction of alginate single-chain polyguluronate segments with mono- and divalent metal cations: A comparative molecular dynamics study. *Molecular Simulation, 36*(10), 778–795. https://doi.org/10.1080/08927021003752853

Qian, C., Asdjodi, M. R., Spencer, H. G., & Savitsky, G. B. (1989). Sodium-23 NMR study of competitive binding of ions to polyelectrolytes in mixed counterion systems. *Macromolecules, 22*(2), 995–998. https://doi.org/10.1021/ma00192a078

Riedl, C., Qian, C., Savitsky, G. B., Spencer, H. G., & Moss, W. F. (1989). Mathematical modeling of the concentration dependence of competitive binding of counterions in polyelectrolytes. *Macromolecules, 22*(10), 3983–3986. https://doi.org/10.1021/ma00200a029

Rolland, L., Santanach-Carreras, E., Delmas, T., Bibette, J., & Bremond, N. (2014). Physicochemical properties of aqueous core hydrogel capsules. *Soft Matter, 10*(48), 9668–9674. https://doi.org/10.1039/C4SM02012J

Sato, T., Norisuye, T., & Fujita, H. (1984). Double-stranded helix of xanthan: Dimensional and hydrodynamic properties in 0.1 M aqueous sodium chloride. *Macromolecules, 17*(12), 2696–2700. https://doi.org/10.1021/ma00142a043

Seale, R., Morris, E. R., & Rees, D. A. (1982). Interactions of alginates with univalent cations. *Carbohydrate Research, 110*(1), 101–112. https://doi.org/10.1016/0008-6215(82)85029-5

Secchi, E., Roversi, T., Buzzaccaro, S., Piazza, L., & Piazza, R. (2013). Biopolymer gels with "physical" cross-links: Gelation kinetics, aging, heterogeneous dynamics, and macroscopic mechanical properties. *Soft Matter, 9*(15), 3931–3944. https://doi.org/10.1039/C3SM27153F

Senturk Parreidt, T., Müller, K., & Schmid, M. (2018). Alginate-based edible films and coatings for food packaging applications. *Foods, 7*(10). https://doi.org/10.3390/foods7100170

Sikorski, P., Mo, F., Skjåk-Bræk, G., & Stokke, B. T. (2007). Evidence for egg-box-compatible interactions in calcium−alginate gels from fiber X-ray diffraction. *Biomacromolecules, 8*(7), 2098–2103. https://doi.org/10.1021/bm0701503

Skjåk-Bræk, G., Grasdalen, H., & Smidsrød, O. (1989). Inhomogeneous polysaccharide ionic gels. *Carbohydrate Polymers, 10*(1), 31–54. https://doi.org/10.1016/0144-8617(89)90030-1

Skjåk-Bræk, G., Smidsrød, O., & Larsen, B. (1986). Tailoring of alginates by enzymatic modification in vitro. *International Journal of Biological Macromolecules, 8*(6), 330–336. https://doi.org/10.1016/0141-8130(86)90051-6

Skolnick, J., & Fixman, M. (1977). Electrostatic persistence length of a wormlike polyelectrolyte. *Macromolecules, 10*(5), 944–948. https://doi.org/10.1021/ma60059a011

Smidsrød, O. (1974). Molecular basis for some physical properties of alginates in the gel state. *Faraday Discussions of the Chemical Society, 57*(0), 263–274. https://doi.org/10.1039/DC9745700263

Smidsrød, O., Glover, R. M., & Whittington, S. G. (1973). The relative extension of alginates having different chemical composition. *Carbohydrate Research, 27*(1), 107–118. https://doi.org/10.1016/S0008-6215(00)82430-1

Smidsrød, O., & Haug, A. (1971). Estimation of the relative stiffness of the molecular chain in polyelectrolytes from measurements of viscosity at different ionic strengths. *Biopolymers, 10*(7), 1213–1227. https://doi.org/10.1002/bip.360100711

Smidsrød, O., & Haug, A. (1972). Properties of poly(1,4-hexuronates) in the gel state II. Comparison of gels of different composition. *Acta Chemica Scandinavica, 26*, 79–88.

Solberg, A., Draget, K. I., Schatz, C., & Christensen, B. E. (2023). Alginate blocks and block polysaccharides: A review. *Macromolecular Symposia, 408*(1), 2200072. https://doi.org/10.1002/masy.202200072

Solberg, A., Mo, I. V., Aachmann, F. L., Schatz, C., & Christensen, B. E. (2021). Alginate-based diblock polymers: Preparation, characterization and ca-induced self-assembly. *Polymer Chemistry, 12*(38), 5412–5425. https://doi.org/10.1039/D1PY00727K

Solberg, A., Mo, I. V., Omtvedt, L. A., Strand, B. L., Aachmann, F. L., Schatz, C., & Christensen, B. E. (2022). Click chemistry for block polysaccharides with dihydrazide and dioxyamine linkers - a review. *Carbohydrate Polymers, 278*, Article 118840. https://doi.org/10.1016/j.carbpol.2021.118840

Stewart, M. B., Gray, S. R., Vasiljevic, T., & Orbell, J. D. (2014a). Exploring the molecular basis for the metal-mediated assembly of alginate gels. *Carbohydrate Polymers, 102*, 246–253. https://doi.org/10.1016/j.carbpol.2013.11.034

Stewart, M. B., Gray, S. R., Vasiljevic, T., & Orbell, J. D. (2014b). The role of poly-M and poly-GM sequences in the metal-mediated assembly of alginate gels. *Carbohydrate Polymers, 112*, 486–493. https://doi.org/10.1016/j.carbpol.2014.06.001

Stokke, B. T., Elgsaeter, A., Skjåk-Bræk, G., & Smidsrød, O. (1987). The molecular size and shape of xanthan, xylinan, bronchial mucin, alginate, and amylose as revealed by electron microscopy. *Carbohydrate Research, 160*, 13–28. https://doi.org/10.1016/0008-6215(87)80300-2

Stokke, B. T., Smidsrød, O., & Brant, D. A. (1993). Predicted influence of monomer sequence distribution and acetylation on the extension of naturally occurring alginates. *Carbohydrate Polymers, 22*(1), 57–66. https://doi.org/10.1016/0144-8617(93)90166-2

Stokke, B. T., Smidsrød, O., Bruheim, P., & Skjåk-Bræk, G. (1991). Distribution of uronate residues in alginate chains in relation to alginate gelling properties. *Macromolecules, 24*(16), 4637–4645. https://doi.org/10.1021/ma00016a026

Stokke, B. T., Smidsrød, O., Zanetti, F., Strand, W., & Skjåk-Bræk, G. (1993). Distribution of uronate residues in alginate chains in relation to alginate gelling properties — 2: Enrichment of β-d-mannuronic acid and depletion of α-l-guluronic acid in sol fraction. *Carbohydrate Polymers, 21*(1), 39–46. https://doi.org/10.1016/0144-8617(93)90115-K

Storz, H., Müller, K. J., Ehrhart, F., Gómez, I., Shirley, S. G., Gessner, P., … Zimmermann, U. (2009). Physicochemical features of ultra-high viscosity alginates. *Carbohydrate Research, 344*(8), 985–995. https://doi.org/10.1016/j.carres.2009.02.016

Strand, B. L., Mørch, Y. A., Espevik, T., & Skjåk-Bræk, G. (2003). Visualization of alginate–poly-L-lysine–alginate microcapsules by confocal laser scanning microscopy. *Biotechnology and Bioengineering, 82*(4), 386–394. https://doi.org/10.1002/bit.10577

Strand, B. L., Mørch, Y. A., Syvertsen, K. R., Espevik, T., & Skjåk-Bræk, G. (2003). Microcapsules made by enzymatically tailored alginate. *Journal of Biomedical Materials Research Part A, 64A*(3), 540–550. https://doi.org/10.1002/jbm.a.10337

Thiviya, P., Gamage, A., Liyanapathiranage, A., Makehelwala, M., Dassanayake, R. S., Manamperi, A., … Madhujith, T. (2023). Algal polysaccharides: Structure, preparation and applications in food packaging. *Food Chemistry, 405*, Article 134903. https://doi.org/10.1016/j.foodchem.2022.134903

Thom, D., Grant, G. T., Morris, E. R., & Rees, D. A. (1982). Characterisation of cation binding and gelation of polyuronates by circular dichroism. *Carbohydrate Research, 100*(1), 29–42. https://doi.org/10.1016/S0008-6215(00)81023-X

Thu, B., Bruheim, P., Espevik, T., Smidsrød, O., Soon-Shiong, P., & Skjåk-Bræk, G. (1996). Alginate polycation microcapsules: II. Some functional properties. *Biomaterials, 17*(11), 1069–1079. https://doi.org/10.1016/0142-9612(96)85907-2

Thu, B., Gåserød, O., Paus, D., Mikkelsen, A., Skjåk-Bræk, G., Toffanin, R., Vittur, F., & Rizzo, R. (2000). Inhomogeneous alginate gel spheres: An assessment of the polymer gradients by synchrotron radiation-induced x-ray emission, magnetic resonance microimaging, and mathematical modeling. *Biopolymers, 53*(1), 60–71. https://doi.org/10.1002/(SICI)1097-0282(200001)53:1<60::AID-BIP6>3.0.CO;2-F

Thumbs, J., & Kohler, H.-H. (1996). Capillaries in alginate gel as an example of dissipative structure formation. *Chemical Physics, 208*(1), 9–24. https://doi.org/10.1016/0301-0104(96)00031-6

Topuz, F., Henke, A., Richtering, W., & Groll, J. (2012). Magnesium ions and alginate do form hydrogels: A rheological study. *Soft Matter, 8*(18), 4877–4881. https://doi.org/10.1039/C2SM07465F

Treloar, L. R. G. (2005). *The physics of rubber elasticity* (3rd ed.). Clarendon Press.

Turco, G., Donati, I., Grassi, M., Marchioli, G., Lapasin, R., & Paoletti, S. (2011). Mechanical spectroscopy and relaxometry on alginate hydrogels: A comparative analysis for structural characterization and network mesh size determination. *Biomacromolecules, 12*(4), 1272–1282. https://doi.org/10.1021/bm101556m

Vold, I. M. N., Kristiansen, K. A., & Christensen, B. E. (2006). A study of the chain stiffness and extension of alginates, in vitro epimerized alginates, and periodate-oxidized alginates using size-exclusion chromatography combined with light scattering and viscosity detectors. *Biomacromolecules, 7*(7), 2136–2146. https://doi.org/10.1021/bm060099n

Wang, Z.-Y., Zhang, Q.-Z., Konno, M., & Saito, S. (1993). Sol–gel transition of alginate solution by the addition of various divalent cations: 13C-nmr spectroscopic study. *Biopolymers, 33*(4), 703–711. https://doi.org/10.1002/bip.360330419

Yamamoto, K., Yuguchi, Y., Stokke, B. T., Sikorski, P., & Bassett, D. C. (2019). Local structure of Ca2+ alginate hydrogels gelled via competitive ligand exchange and measured by small angle X-ray scattering. *Gels, 5*(1). https://doi.org/10.3390/gels5010003

Yang, J., & Sato, T. (2020). Conformation of pullulan in aqueous solution studied by small-angle X-ray scattering. *Polymers, 12*(6). https://doi.org/10.3390/polym12061266